Mineralogy, morphology, and emplacement history of the Maaz formation on the Jezero crater floor from orbital and rover observations

Briony Heather Noelle Horgan[1], Arya Udry[2], Meiissa S Rice[3], Sanna Alwmark[4], Hans E. F. Amundsen[5], James F. Bell III[6], Larry S. Crumpler[7], Bradley Garczynski[1], Jeffrey R. Johnson[8], Kjartan Münster Kinch[9], Lucia Mandon[10], Marco Merusi[9], Chase Million[11], Jorge I. Núñez[8], Patrick S. Russell[12], Justin I. Simon[13], Michael St. Clair[11], Kathryn Stack Morgan[14], Alicia Fallacaro Vaughan[15], Brittan Valhalla Wogsland[16], Andrew Michael Annex[17], Andreas Bechtold[18], Tor Berger[19], Olivier Beyssac[20], Adrian Jon Brown[21], Edward Cloutis[22], Barbara A Cohen[23], Sarah Fagents[24], Linda C Kah[25], Ken Farley[17], David Timothy Flannery[26], Sanjeev Gupta[27], Sein-Erik Hamran[19], Yang Liu[28], Gerhard Paar[29], Cathy Quantin-Nataf[10], Nicolas Randazzo[30], Eleni Maria Ravanis[31], Steven F Sholes[14], David Shuster[32], Vivian Zheng Sun[14], Christian Tate[33], Nicholas Tosca[34], Meenakshi Wadhwa[6], and Roger C. Wiens[35]

[1]Purdue University
[2]Department of Geoscience, University of Nevada, Las Vegas
[3]Western Washington University
[4]Niels Bohr Institute, University of Copenhagen
[5]Earth and Planetary Exploration Services
[6]Arizona State University
[7]New Mexico Museum of Natural History
[8]Johns Hopkins University Applied Physics Laboratory
[9]University of Copenhagen
[10]Laboratoire de Géologie de Lyon
[11]Million Concepts
[12]UCLA
[13]Center for Isotope Cosmochemistry and Geochronology, Astromaterials Research and Exploration Science, NASA Johnson Space Center
[14]Jet Propulsion Laboratory
[15]Apogee Engineering, LLC
[16]University of Tennessee
[17]California Institute of Technology
[18]Department of Lithospheric Research
[19]University of Oslo
[20]Institut de Minéralogie, de Physique des Matériaux et de Cosmochimie (IMPMC), Université Pierre-et-Marie-Curie (UPMC)
[21]Plancius Research
[22]University of Winnepeg

[23]University of New Mexico
[24]Hawai'i Institute of Geophysics and Planetology, University of Hawai'i at Mānoa
[25]University of Tennessee at Knoxville
[26]Science and Engineering Faculty, Queensland University of Technology
[27]Imperial College
[28]Jet Propulsion Laboratory, California Institute of Technology
[29]JOANNEUM RESEARCH
[30]Department of Earth and Atmospheric Sciences, University of Alberta
[31]Department of Earth Sciences, University of Hawai'i, Honolulu, HI, USA
[32]Unknown
[33]Cornell University
[34]University of Cambridge
[35]Los Alamos National Laboratory (DOE)

January 20, 2023

Abstract

The first samples collected by the Perseverance rover on the Mars 2020 mission were from the Maaz formation, a lava plain that covers most of the floor of Jezero crater. Laboratory analysis of these samples back on Earth will provide important constraints on the petrologic history, aqueous processes, and timing of key events in Jezero. However, interpreting these samples will require a detailed understanding of the emplacement and modification history of the Maaz formation. Here we synthesize rover and orbital remote sensing data to link outcrop-scale interpretations to the broader history of the crater, including Mastcam-Z mosaics and multispectral images, SuperCam chemistry and reflectance point spectra, RIMFAX ground penetrating radar, and orbital hyperspectral reflectance and high-resolution images. We show that the Maaz formation is composed of a series of distinct members corresponding to basaltic to basaltic andesite lava flows. The members exhibit variable spectral signatures dominated by high-Ca pyroxene, Fe-bearing feldspar, and hematite, which can be tied directly to igneous grains and altered matrix in abrasion patches. Spectral variations correlate with morphological variations, from recessive layers that produce a regolith lag in lower Maaz, to weathered polygonally fractured paleosurfaces and crater-retaining massive blocky hummocks in upper Maaz. The Maaz members were likely separated by one or more extended periods of time, and were subjected to variable erosion, burial, exhumation, weathering, and tectonic modification. The two unique samples from the Maaz formation are representative of this diversity, and together will provide an important geochronological framework for the history of Jezero crater.

Hosted file

`essoar.10512674.1.docx` available at https://authorea.com/users/531790/articles/620328-mineralogy-morphology-and-emplacement-history-of-the-maaz-formation-on-the-jezero-crater-floor-from-orbital-and-rover-observations

Mineralogy, morphology, and emplacement history of the Maaz formation on the Jezero crater floor from orbital and rover observations

Submitted to Journal of Geophysical Research - Planets

Briony Horgan*[1], Arya Udry[2], Melissa Rice[3], Sanna Alwmark[4,5], Hans Amundsen[6], Jim Bell[7], Larry Crumpler[8], Brad Garczynski[1], Jeff Johnson[9], Kjartan Kinch[5], Lucia Mandon[10], Marco Merusi[5], Chase Million[11], Jorge I. Núñez[9], Patrick Russell[12], Justin I. Simon[13], Michael St. Clair[11], Katie Stack-Morgan[14], Alicia Vaughan[15], Brittan Wogsland[16], Andrew Annex[17,18], Andreas Bechtold[19,20], Tor Berger[6], Olivier Beyssac[21], Adrian Brown[22], Ed Cloutis[23], Barbara A. Cohen[24], Sarah Fagents[25], Linda Kah[16], Ken Farley[17], David Flannery[26], Sanjeev Gupta[27], Svein-Erik Hamran[6], Yang Liu[14], Gerhard Paar[28], Cathy Quantin-Nataf[29], Eleni Ravanis[25], Nicolas Randazzo[30], Steven Sholes[14], David Shuster[31], Vivian Sun[14], Christian Tate[32], Nick Tosca[33], Mini Wadhwa[7], Roger C. Wiens[1]

*Corresponding author (briony@purdue.edu)

[1]Department of Earth, Atmospheric, and Planetary Sciences, Purdue University, West Lafayette, IN 47906. [2]Department of Geosciences, University of Nevada Las Vegas, Las Vegas, NV 89123. [3]Western Washington Univ. [4]Department of Geology, Lund University, Sölvegatan 12, 22362 Lund, Sweden. [5]Niels Bohr Institute, University of Copenhagen, 2100 Copenhagen, Denmark. [6]Center for Space Sensors and Systems (CENSSS), University of Oslo. [7]School of Earth and Space Exploration, Arizona State University, Tempe AZ 85287. [8]New Mexico Museum of Natural History and Science, Albuquerque, NM 87120. [9]Johns Hopkins University Applied Physics Laboratory, Laurel, MD 20723. [10]LESIA, Observatoire de Paris, Université PSL, CNRS, Sorbonne Université, Université de Paris, Meudon, France. [11]Million Concepts LLC. [12]Dept. EPSS, University of California at Los Angeles, Los Angeles CA 90095. [13]Center for Isotope Cosmochemistry and Geochronology, Astromaterials Research and Exploration Science, NASA Johnson Space Center, Houston, TX. [14]Jet Propulsion Laboratory, California Institute of Technology, Pasadena, CA 91109. [15]Apogee Engineering, LLC. [16]Department of Earth and Planetary Sciences, University of Tennessee, Knoxville, TN 37996 . [17]Division of Geological and Planetary Sciences, California Institute of Technology, Pasadena, CA, 91125. [18]Morton K. Blaustein Department of Earth & Planetary Sciences, Johns Hopkins University, Baltimore, MD, 21218. [19]Department of Lithospheric Research, University of Vienna, 1090 Vienna, Austria. [20]Austrian Academy of Sciences, 1010 Vienna, Austria. [21]Institut de Minéralogie, de Physique des Matériaux et de Cosmochimie, CNRS, Sorbonne Université, Muséum National d'Histoire Naturelle, 75005 Paris, France. [22]Plancius Reseach, LLC, Severna Park MD 21146. [23]Centre for Terrestrial and Planetary Exploration, University of Winnipeg, Winnipeg, Canada R3B 2E9. [24]NASA Goddard Space Flight Center, Greenbelt MD 20771. [25]Hawai'i Institute of Geophysics and Planetology, University of Hawai'i at Mānoa Honolulu, HI 96822. [26]Queensland University of

Technology, Brisbane, Queensland, Australia. [27]*Department of Earth Science and Engineering, Imperial College London, London SW72AZ, United Kingdom* [28]*JOANNEUM RESEARCH, Institute for Information and Communication Technologies, Austria.* [29]*Laboratoire de Géologie de Lyon: Terre, Planètes, Environnement, Université de Lyon, Université Claude Bernard Lyon1, Ecole Normale Supérieure de Lyon, Université Jean Monnet Saint Etienne, CNRS, 69100 Villeurbanne, France.* [30]*Department of Earth and Atmospheric Sciences, University of Alberta, Edmonton, AB T6G 2R3.* [31]*Department of Earth and Planetary Science, University of California, Berkeley, CA 94720-4767.* [32]*Department of Astronomy, Cornell University, Ithaca, NY.* [33]*Department of Earth Sciences, University of Cambridge, Cambridge, CB2 3EQ, United Kingdom*

Key Points

- The Maaz formation is a series of pyroxene and plagioclase-dominated lava flows on the Jezero crater floor with variable morphologies
- Significant erosion and tectonism occurred during at least one flow hiatus, suggesting emplacement over an extended period of time
- The crystallization ages of Maaz formation samples will help constrain the timing of delta activity and the global cratering chronology

Abstract

The first samples collected by the Perseverance rover on the Mars 2020 mission were from the Maaz formation, a lava plain that covers most of the floor of Jezero crater. Laboratory analysis of these samples back on Earth will provide important constraints on the petrologic history, aqueous processes, and timing of key events in Jezero. However, interpreting these samples will require a detailed understanding of the emplacement and modification history of the Maaz formation. Here we synthesize rover and orbital remote sensing data to link outcrop-scale interpretations to the broader history of the crater, including Mastcam-Z mosaics and multispectral images, SuperCam chemistry and reflectance point spectra, RIMFAX ground penetrating radar, and orbital hyperspectral reflectance and high-resolution images. We show that the Maaz formation is composed of a series of distinct members corresponding to basaltic to basaltic andesite lava flows. The members exhibit variable spectral signatures dominated by high-Ca pyroxene, Fe-bearing feldspar, and hematite, which can be tied directly to igneous grains and altered matrix in abrasion patches. Spectral variations correlate with morphological variations, from recessive layers that produce a regolith lag in lower Maaz, to weathered polygonally fractured paleosurfaces and crater-retaining massive blocky hummocks in upper Maaz. The Maaz members were likely separated by one or more extended periods of time, and were subjected to variable erosion, burial, exhumation, weathering, and tectonic modification. The two unique samples from the Maaz formation are representative of this diversity, and together will provide an important geochronological framework for

the history of Jezero crater.

Plain language summary:

The Perseverance rover on the Mars 2020 mission is collecting samples from Jezero crater for eventual return to Earth via Mars Sample Return, and the first samples collected by the rover were from the Maaz formation, a lava plain that covers much of the crater floor. These igneous samples can be used to date when the lavas crystallized and to better understand their later interactions with water, both of which will be important for reconstructing the history of habitable environments in Jezero. In this study we use images and reflectance spectra from the rover and orbiters, along with ground penetrating radar from the rover, to determine the history of the Maaz formation lavas. We find evidence for significant erosion and weathering in between successive flows, suggesting that they were emplaced over a long period of time. Some of the lavas underlie the Jezero delta, and so their age will provide limits on the timing of lake activity in Jezero, while others retain craters, so their age will help to better understand crater density-based age estimates for surfaces across Mars.

1. Introduction

The Perseverance rover on the Mars 2020 mission is collecting samples from Jezero crater, a Noachian impact crater that has experienced a complex history of igneous, aqueous, and aeolian processes (Farley et al., 2020), for eventual return to Earth. Two of the four unique rock samples acquired by Perseverance on the Jezero crater floor were extracted from the Maaz formation, which from orbit corresponds to a rough unit with lobate margins that appears to embay local topography (Figure 1). Morphologic and petrologic observations of the Maaz formation by Perseverance are most consistent with a series of lava flows (Farley et al., 2022; Alwmark et al., this issue; Udry et al. this issue; Crumpler et al., this issue), confirming some hypotheses based on orbital data that the unit is igneous in origin (Schon et al., 2012; Goudge et al., 2015; Horgan et al., 2020a, Stack and Sun, 2020).

The Maaz formation ("Máaz" is the Navajo name for Mars) provides an important stratigraphic and geochronological link between other major geologic units in Jezero crater. The Maaz formation overlies the Seitah formation ("Séítah" is Navajo for "amidst the sands"), which is a layered and eroded landscape of ridges and sand that is interpreted as an olivine-dominated cumulate likely originating in a thick lava flow or lava lake that once filled the crater floor (Liu et al., 2022). The western delta and other sedimentary remnants in Jezero appear to overlie the Maaz formation (Alwmark et al., 2021), suggesting that some or all lacustrine activity post-dated emplacement of crater floor lavas. Geochronological analyses of these samples back on Earth may thus provide critical constraints on the timing of events in Jezero crater, including emplacement of the crater floor as well as potentially the onset of lake activity (Simon et al., this issue).

Crater densities on the Maaz formation may also provide important constraints on interpretations of the global martian crater chronology, if the surface's erosional, burial, and exhumation history can be constrained. However, additional geologic context from rover and orbital datasets is needed to understand how the Maaz formation fits into the regional history.

In this paper, we tie in situ observations from Perseverance to orbital data to understand the emplacement history and geochronological significance of the Maaz formation. We seek to understand the relationships between stratigraphic members in outcrop and how these members relate to morphologies and spectral properties observed from orbit, in order to develop a framework for the emplacement history of crater floor rocks and their relationship to the delta. We investigate the compositional and morphological diversity of stratigraphic members within the Maaz formation as observed by Perseverance using Mastcam-Z multispectral images supported by SuperCam reflectance spectra and elemental chemistry as well as RIMFAX ground penetrating radar, and compare these results to orbital data from the CRISM imaging spectrometer and the HiRISE camera.

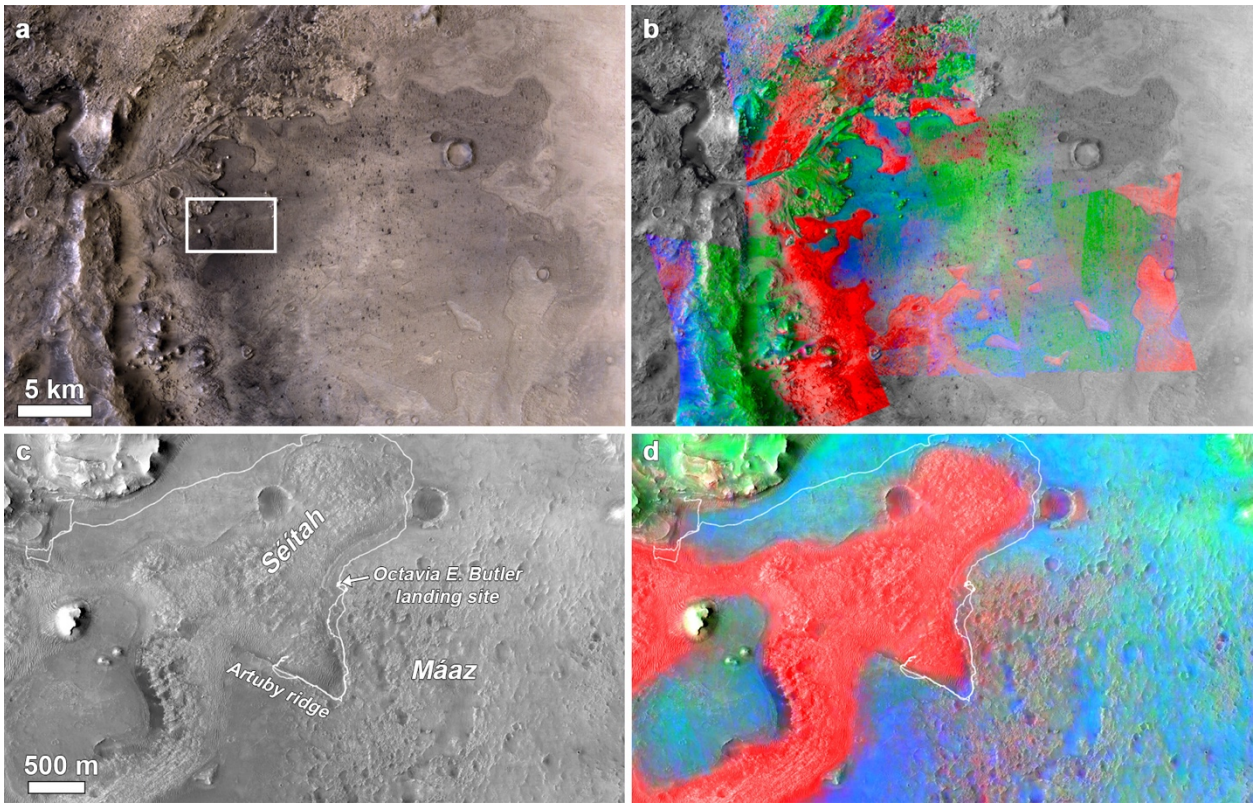

Figure 1: *Overview of Jezero crater floor. (a) Colorized CTX mosaic showing lobate margins of Maaz formation. (b) CRISM mafic parameter combi-*

nation over HiRISE mosaic, where red, green, and blue indicate olivine-like, orthopyroxene-like, and clinopyroxene spectral signatures. The Maaz formation is dominated by pyroxene spectral signatures, in contrast to the olivine signatures of the Seitah formation. (c-d) Zoom on the region of Perseverance's traverse, which shows more diversity at local scales in Maaz.

2. Methods

2.1 Mastcam-Z

Mastcam-Z (Mast camera-Zoom; Bell et al., 2020) is a pair of mast-mounted cameras on the Perseverance rover that have adjustable focal lengths equipped with CCD detectors with bonded Bayer-pattern broadband filters at red/green/blue wavelengths (630/544/480 nm). Each camera is also equipped with a filter wheel with additional narrowband filters, enabling multispectral imaging across the visible /near-infrared (VNIR; 442-1022 nm) at 14 unique wavelengths (Hayes et al., 2021). Mastcam-Z images are calibrated to radiance factor (I/F; where I is the scene radiance and F is the solar irradiance) using near-simultaneous observations of a calibration target mounted on the rover deck (Kinch et al., 2020; Merusi et al., this issue) and pre-flight calibration coefficients (Hayes et al., 2021). Spectra are then converted to relative reflectance (R*) by dividing by the cosine of the solar incidence angle.

Mastcam-Z acquired >300 multispectral images as well as ~300 landscape mosaics during the crater floor campaign (sols 0-380) and the following "rapid traverse" over the crater floor to the delta (sols 381-409; Sun et al., this issue). Spectral diversity was assessed in multispectral images using false-color combinations, decorrelation stretches, and spectral parameter maps (Rice et al., 2022a, this issue). Representative bedrock spectra were extracted from approximately co-located regions of interest (ROIs) in images from both left and right cameras, and collected into a database along with key image metadata (Rice et al. 2022b; St. Clair et al., this issue). We focus on in situ multispectral data taken by Mastcam-Z of dark rock surfaces that are relatively dust-free and without evidence for significant coverage by the purple coatings that are common throughout the crater floor (Garczynski et al., this issue). The work presented here complements and is informed by more detailed analyses of the Mastcam-Z multispectral dataset on the Jezero crater floor (Rice et al., this issue).

2.2 SuperCam

SuperCam measures rock chemistry via Laser-Induced Breakdown Spectroscopy (LIBS), which uses a pulsed 1064 nm laser beam to create a plasma from the target rock or soil, which is analyzed between 245 to 853 nm, with a field of view (FOV) of ~0.8 mrad. Geochemical analyses can be conducted with targets located from 1.5 to ~11 m, with a laser beam of ~170 µm diameter at 2.4 m and ~370 m at 5.5 m (Maurice et al., 2021, Wiens et al., 2021). Most

observations include 30 shots, with the first five shots removed as they likely represent the dust layer (Maurice et al., 2021). We selected the best LIBS data (Udry et al., this issue) from natural rock surfaces with distance <6.5 meters, focus (two consecutive autofocus fit curves performed during a raster are separated by less than 18 steps of the focus motor stage), and intensity ($>10^{14}$ photons/pulse/mm^2/sr/nm at the source). The points with low major-element oxide (eight elements; MOC) totals (< 80 wt.%), were removed as they would indicate missing chemical species (e.g., OH, SO_4^{2-}, CO_3^{2-}), likely associated with secondary phases. We averaged the LIBS data for each member (Artuby, Rochette, Roubion, Nataani, Chal, Content, Seitah) to retrieve approximate bulk chemistries.

SuperCam also acquires reflectance spectra of surfaces in the visible and near-infrared (VISIR) using a transmission spectrometer covering the 535-855 nm range in 6000 channels and an acousto-optic tunable filter (AOTF) spectrometer covering the 1.3-2.6 µm range in 256 channels. The field of view of the instrument is 0.7 mrad in the visible range and 1.15 mrad in the near-infrared (Maurice et al., 2021), which corresponds to a few mm-wide analytical footprints for targets in the rover workspace. During the crater floor campaign, SuperCam measured more than 1500 VISIR spectra on rock targets and allowed the in situ detection of a wide range of minerals on the crater floor (e.g., olivine, pyroxene, oxyhydroxides, phyllosilicates, carbonates and sulfates; Mandon et al., this issue). Here, individual point spectra acquired on rock targets (both unabraded and abraded) were averaged for each specific member of the Maaz formation, excluding observations with saturation or major shadowing in the field of view.

2.3 RIMFAX

The Radar Imager for Mars' subsurface eXperiment (RIMFAX; Hamran et al., 2020) ground penetrating radar (GPR) measures the shallow subsurface beneath the rover's path. Radar reflections indicate changes in permittivity related to changes in density or composition, which often correlate with changes in lithology that can be used to infer stratigraphy. Here we used RIMFAX subsurface soundings to test our stratigraphic models developed based on surface outcrops imaged by Mastcam-Z.

The RIMFAX radar uses a gated Frequency Modulated Continuous Wave (FMCW) waveform over a range of 150 MHz to 1200 MHz. Soundings are collected every 10 cm along the rover traverse. At each location, three primary sounding modes are collected, each focusing on a different zone of the subsurface: Surface, Shallow, Deep. This partitioning is accomplished by varying the gating, time-delay, gain, and processing. As with any GPR, transmitted waves propagate downward until they are reflected back by shallow subsurface interfaces in geologic materials or structures, across which discontinuities in permittivity exist. The raw location of each sounding is given by surface attitude position and pointing (SAPP) software on the rover, which is fit between traverse end points localized by the M2020 localization

team. Radargrams used here display the absolute value of the complex signal value. Depth is estimated from time-delay with a constant subsurface velocity of 0.1 m/ns, consistent with typical permittivities measured from subsurface hyperbolas in RIMFAX data (Casademont et al., 2022)

2.4 Orbital datasets

Variations in surface texture across the crater floor were assessed using HiRISE (High Resolution Imaging System; McEwen et al., 2007) high-resolution grayscale images (25-50 cm/pixel). Mineralogical variations were assessed using reflectance spectra from the CRISM (Compact Reconnaissance Imaging Spectrometer for Mars; Murchie et al., 2007) hyperspectral imaging spectrometer (350-2600 nm; ~18-36 m/pixel). CRISM mapped targeted reduced data records (MTRDR) on the NASA Planetary Data System have been processed to suppress atmospheric and instrumental effects (Seelos et al., 2016) and include a set of pre-calculated spectral parameters, derived from I/F cubes and refined to reduce noise (Viviano-Beck et al., 2014). RGB composites were generated from these spectral parameters to evaluate spectral diversity across the crater floor, which was verified using detailed spectral analysis and comparison to laboratory endmembers. Estimated Lambert albedo spectra were extracted from the MTRDR's and ratioed with spectrally neutral terrains to bring out subtle spectral features. Ratio spectra were extracted from cubes processed as described in Horgan et al. (2020a).

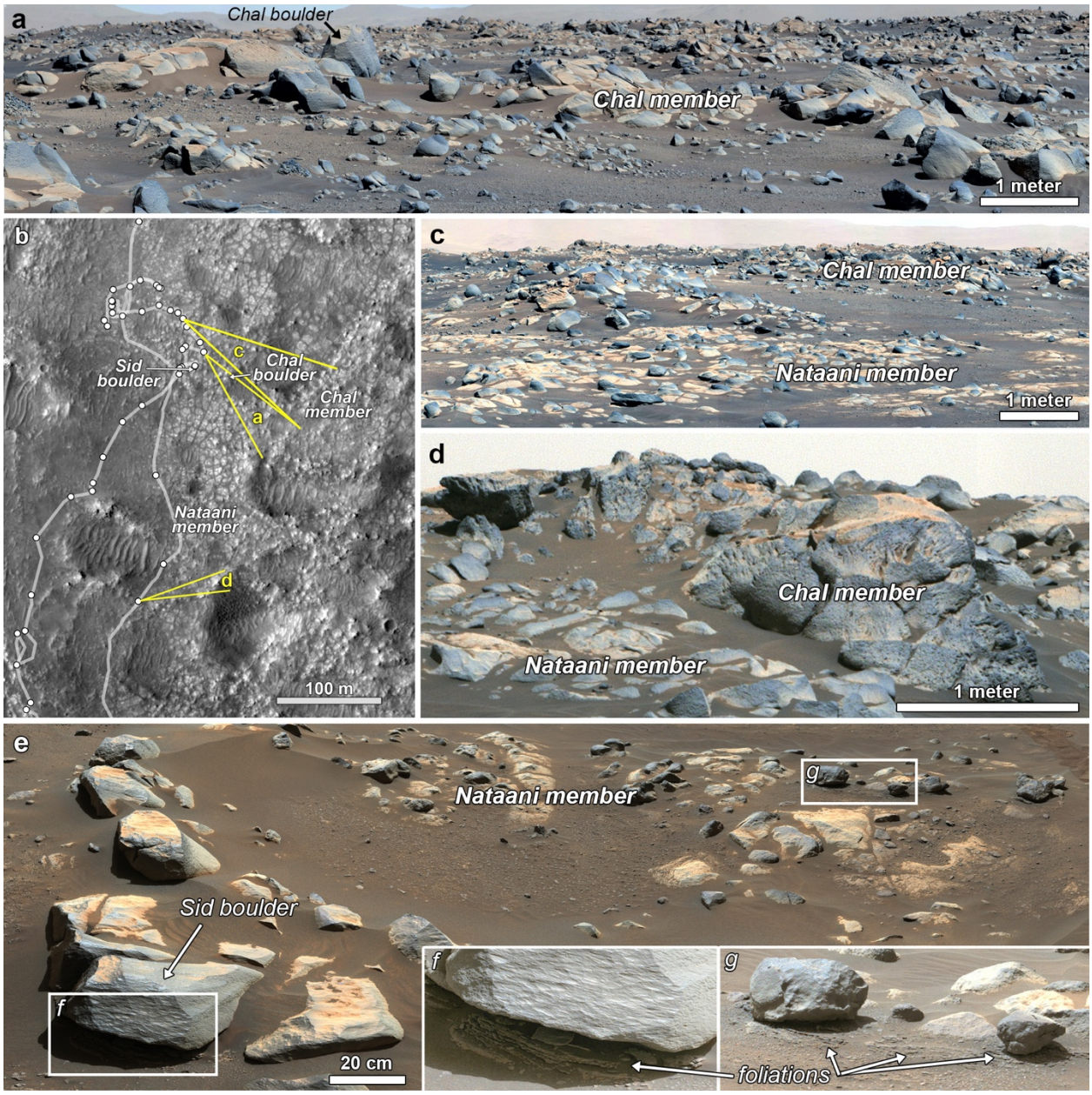

Figure 2: *Chal and Nataani outcrop mophologies near the Octavia E. Butler landing site. (a) Boulders and hummocks of the Chal member from Mastcam-Z (sol 78 zcam08041) and (b) from HiRISE (ESP…). (c) Massive vesicular Chal outcrops at the edge of the roughest zomes (sol 357 zcam08388). (d) Nataani polygonal surfaces transitioning to Chal boulders (sol 64 zcam08109). (e) Sid block of the Chal member, where the Hahonih and Atsah samples were acquired*

(sol 364 zcam08396), overlying Nataani benches and (f) foliations that are visible in a contrast enhanced image (sol 53 zcam08100).

3. Morphology

3.1 Orbital context

From orbit, the upper surface of the crater floor is defined by distinctive lobate margins in most locations, and most commonly, a rough, fractured, and cratered appearance with variable regolith cover (Figure 1c). This unit, previously mapped as the "Crater floor - fractured rough" (Cf-fr) unit of Stack et al. (2020), appears to overlie and embay a ridged and layered unit mapped as "Crater floor - fractured 1" (Cf-f-1). The region of Cf-fr explored by Perseverance has been named the Maaz formation. Perseverance remote sensing and radar observations confirm that Cf-fr/Maaz overlies Cf-f-1 (Farley et al., 2022), which has been named the Seitah formation in the region of the traverse, and is interpreted as an eroded olivine cumulate originating in a lava lake or thick lava flow (Liu et al., 2022). Based on the lobate margins, rough texture, and embaying relationships with Cf-f-1, previous studies hypothesized that Cf-fr could be a lava flow, but a pyroclastic or sedimentary origin could not be ruled out based on orbital data alone (Schon et al., 2012; Goudge et al., 2015;, Horgan et al., 2020a; Sun & Stack, 2020).

A more detailed analysis of surface textures in HiRISE images near the traverse and delta reveals that the surface texture of Cf-fr/Maaz is quite variable, and generally falls into four morphotypes: (1) Rough hummocks dominated by large and rounded boulders and often exhibiting impact craters (Figure 2b); (2) Smooth regolith-poor terrains fractured into meter-scale polygons (Figure 3a); (3) Flat fragmented blocks embedded in smooth and dark terrains (Figure 4b); (4) Smooth and dark terrains with large linear or radial fractures. Rough terrains dominate most of the crater floor east of the Mars 2020 landing site, but smooth terrains dominate west and north of the landing site and close to the delta (Figure 1c).

3.2 In situ observations

On the ground, Mastcam-Z images looking east of the landing site show that the rough hummocks are indeed composed of massive boulders (tens of cm to meters in size) and some in place massive outcrop forming local topographic highs (Figure 2a). This terrain is demarcated as the Chal member of the Maaz formation (Ch'ał in Navajo). The largest outcrops and boulders were not encountered at close range, but some smaller boulders along the traverse show possible vesicular textures. No clear layering of any variety was observed within the Chal member. Perseverance abraded and collected a sample from a large block known as Sid that was inferred to be part of the Chal member (Figure 2e).

Near the landing site, Chal member boulders overlie smooth to knobby meter-scale polygonal surfaces that sometimes appear to form local benches, demarcated as the Nataani member (Naat'áanii in Navajo; Figure 2c-e). Some Nataani blocks exhibit sinuous chains of cm-scale pits that may be possible vesicle trains. The Sid block is inferred to preserve the contact between Chal and Nataani, as thin foliations are observed beneath Sid and similar blocks throughout the area (Figure 2f-g). Similar foliations are observed in cross-section at the Mure outcrop ~1 km south of the landing site (Figure 3e), where they more strongly resemble flow banding in igneous rocks (Alwmark et al., this issue). Mure also exhibits pit chains and smooth surfaces at the top of the outcrop that are similar to Nataani, as well as lobate morphologies in outcrop that are consistent with pahoehoe lavas (Figure 3e; Alwmark et al., this issue). No samples or abrasions were conducted on rocks of the Nataani member.

The Mure outcrop forms the southern margin of a 200-300 m wide and 5-10 m deep valley that cuts into the Maaz formation, colloquially known as "Polygon Valley" (Figure 3a), because it is floored by flat-lying, meter-scale polygonal surfaces of the Roubion member (Figures 3b and 3f). This member was not observed in cross section near the rover, but exposed blocks within the member are distinctive, exhibiting a dark tone and pitted and rough texture with subtle layering (Figure 3g). This texture is similar to exposures of dark, pitted, and rough-textured layers exposed in the deepest parts of Polygon Valley to the NE, 200 m from the traverse, suggesting that these may be outcrops of the Roubion member (Figure 3c-d). In this northern part of the valley, the outcrops transition to polygonal surfaces also consistent with Roubion, which together cover an elevation range of up to 8 meters, potentially representing one of the thickest outcrops of an individual member of the Maaz formation observed by Perseverance.

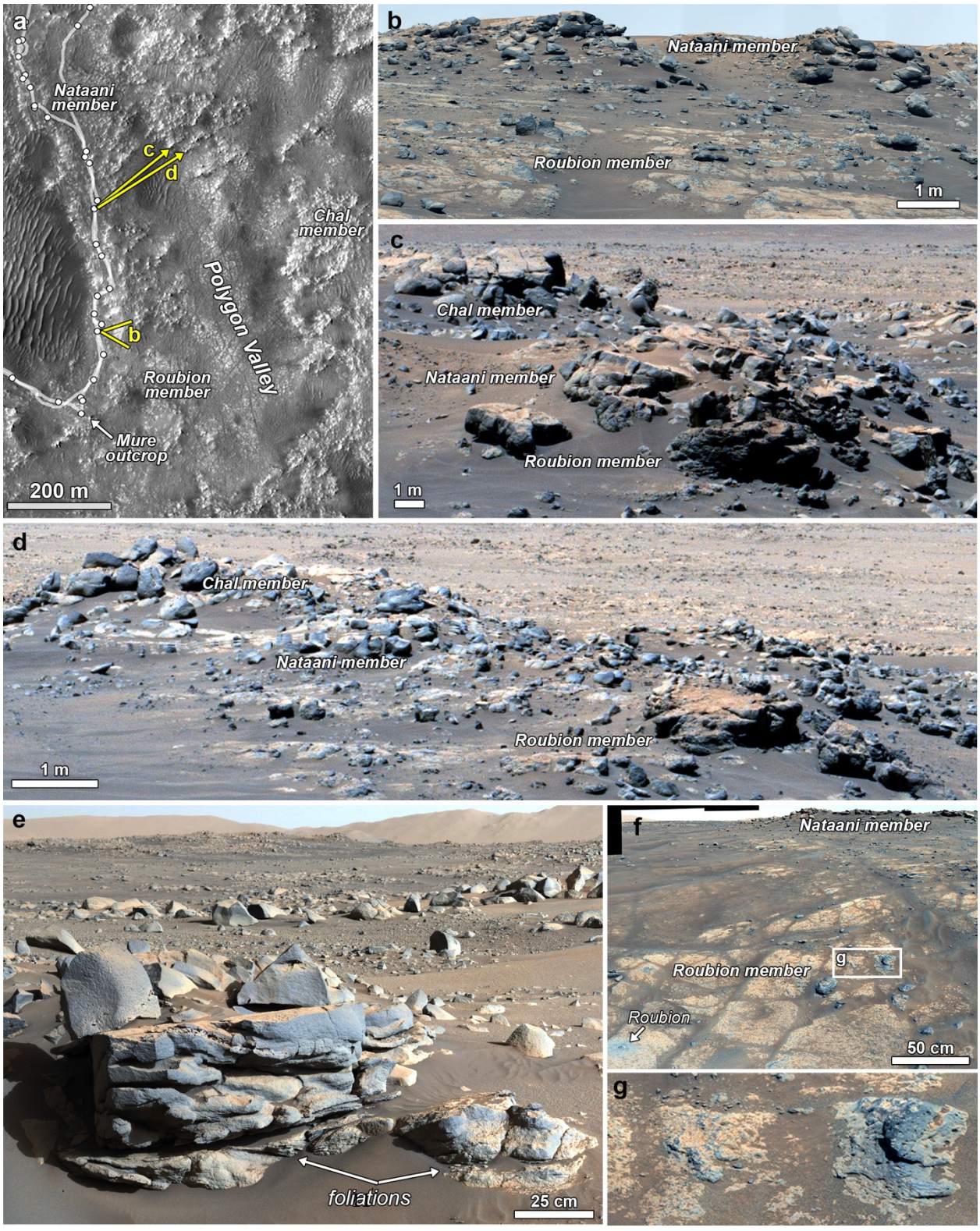
a
Nataani member
c
d
Chal member
Polygon Valley
b
Roubion member
Mure outcrop
200 m
b
Nataani member
Roubion member
1 m
c
Chal member
Nataani member
Roubion member
1 m
d
Chal member
Nataani member
Roubion member
1 m
e
foliations
25 cm
f
Nataani member
g
Roubion member
Roubion
50 cm
g

Figure 3: *Outcrops around Polygon Valley, south of the landing site. (a) HiRISE context view. (b) Entrance to Polygon Valley, showing rough, dark, and pitted Roubion polygons with subtle layering transitioning to a massive layered capping outcrop, interpreted as Nataani (sol 138 zcam08147). (c-d) To the northeast, showing outcrop views of the dark, rough, and pitted Roubion layers overlain by massive layers and boulders, interpreted as Nataani and Chal, respectively (Sol 132 zcam08134). (e) To the south at Mure, a possible outcrop of Nataani member (sol 168 zcam08180), (f-g) which is underlain by dark pitted Roubion member pavers (sol 163 zcam08172).*

The outcrop expression of the Maaz formation changes substantially to the west of Mure at Artuby ridge, along the southern contact with the Seitah formation. Artuby is defined by apparent layers ranging from a few to tens of cm in thickness that dip to the southeast, with variable layer morphology (Alwmark et al., this issue). The sharp ridge top and thus the margin of the Maaz formation at this location is typically characterized by resistant and cliff-forming blocks of the Rochette member (Figure 4e), which in outcrop exhibit linear fabrics resembling planar fractures or joints rather than layers (Figure 4a). Below the resistant Rochette member cap, the Artuby ridge outcrop transitions to knob-forming and rounded or even recessive and friable layers of the Artuby member (Figure 4d and 4g). The surface expression of the plains to the south of Artuby ridge is characterized by exposure of more resistant Rochette layers as fractured blocks, embedded in dark regolith that may be sourced from Rochette or the more friable Artuby layers (Figure 4f). The Rochette member was abraded and sampled in one of these fragmented surface blocks named Rochette (Figure 4f), and the Artuby member was abraded at the Rimplas outcrop (Figure 4g).

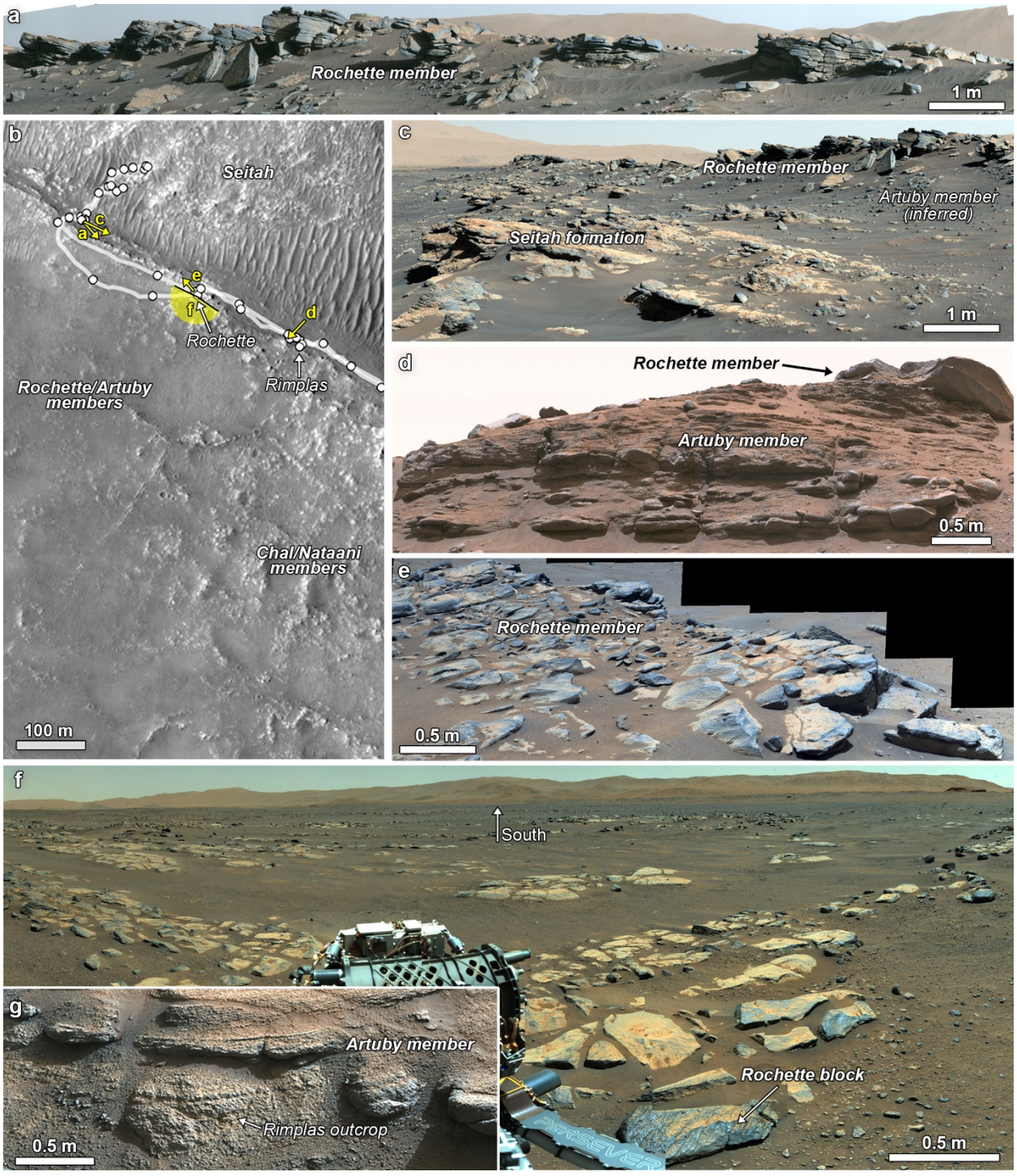
a
Rochette member
1 m
b
Seitah
c
a
e
f
d
Rochette
Rimplas
Rochette/Artuby members
Chal/Nataani members
100 m
c
Rochette member
Artuby member (inferred)
Seitah formation
1 m
d
Rochette member
Artuby member
0.5 m
e
Rochette member
0.5 m
f
South
g
Artuby member
Rimplas outcrop
0.5 m
Rochette block
0.5 m

Figure 4: *Outcrops along Artuby ridge. (a) Rochette mb. resistant cap showing planar jointing (sol 289 zcam08314). (b) Zoom on HiRISE mosaic over Artuby ridge area showing image locations. (c) Tilted beds of the Seitah fm. underlying Rochette and Artuby mb. (sol 305 zcam03281). (d) Thin recessive and thicker knobby resistant layers in the Artuby mb. (sol 342 zcam03309). (e) Overlooking Rochette mb. on ridge top (sol 180 zcam08194). (f) Landscape view looking south of Artuby ridge from Mastcam-Z (sol 181 zcam08199). (g) Outcrop view of Rimplas abrasion target in Artuby mb. (sol 343 zcam07101).*

3.3 Synthesis of orbital and in situ data

The rough hummocks observed from orbit in the Maaz formation appear to correspond to the Chal member, the smooth polygonal surfaces appear to correspond to the Nataani and Roubion members, and the fragmented blocks embedded in smooth terrains appear to correspond to the Rochette/Artuby members. The contrast between the surface expressions of Nataani/Chal and Rochette/Artuby is most apparent to the south of the rover traverse, where the rough landscape south of Mure of boulders and hummocks of Nataani/Chal (Figure 1c) sharply transitions south of Artuby ridge (Figure 4b) to the smooth landscape of fractured blocks and regolith of Rochette/Artuby (Figure 4f).

4. Spectral and chemical properties

4.1 CRISM

One of the clearest distinctions between the Seitah formation and the Maaz formation from orbit is in their spectral signatures, as highlighted in the CRISM mafic RGB combination in Figure 1, where Seitah shows up as red and Maaz as blue to green. Ratioed CRISM spectra in Seitah exhibit a deep and broad band centered between 1.07-1.3 m, with a strong shoulder between 1.3-1.5 m that is attributed to olivine (red spectra in Figure 5). These areas exhibit high BD1300 values, which causes them to show up as bright red in the CRISM mafic RGB combination in Figure 1. Some variability is observed in the shape and position of the band, which could be related to compositional variations in the olivine, but as these variations often correlate with sediment cover, they are instead likely related to variations in grain size in outcrop vs. regolith as well mixing with more diverse regolith materials (Horgan et al., 2020a). Perseverance observations confirm that Seitah bedrock is dominated by mm-size olivine grains in a clinopyroxene matrix (Liu et al., 2022; Wiens et al., 2022; Beyssac et al., this issue), and that surface regolith is a mix of coarse olivine grains and finer pyroxene-dominated grains (Vaughan et al., this issue).

CRISM spectral signatures show a strong correlation with surface morphology in the Maaz formation. Smooth surfaces south of Artuby ridge attributed to the Rochette/Artuby members above exhibit a weaker and more symmetric band centered closer to 1 m, without the strong olivine shoulder (spectra 7-8

in Figure 5a). This band is paired with a broad and shallow band centered near 2.2 m, which is consistent with clinopyroxene (CPX). The specific positions of the bands (most commonly 1.00-1.04 and 2.15-2.20 m) are most consistent with Fe-rich and moderately calcic pyroxenes (e.g. Wo35 Fs65 augite in Figure 5b; Cloutis & Gaffey, 1991a; Klima et al., 2011). Absorption in these spectra between 2.12-2.46 m relative to 1.6 and 2.53 m causes high values of HCPINDEX2, which causes these areas to show up as blue in the CRISM mafic RGB combination in Figure 1. However, at CRISM scales (18-36 m/pixel) it is unclear if these signatures are related to bedrock, surficial regolith, or both.

Rough surfaces, including those attributed to the Chal/Nataani members above, do not exhibit a 2 m band that would suggest the presence of most common pyroxenes (Cloutis & Gaffey, 1991a). Instead, these areas only exhibit a broad and weak band near 1 m, with center positions varying from 1.08-1.20 m (spectra 8-9 in Figure 5a). These areas also often exhibit a weak band at 0.86 m superposed on this broader band, consistent with crystalline hematite. The broad band could be due to olivine, and in some locations can be attributed to olivine in surface regolith. For example, the Perseverance landing site near the margin of Seitah is covered by dark regolith and shows bands consistent with an olivine/pyroxene mixture (spectrum 4 in Figure 5a). However, elsewhere in the Maaz formation the broad band is associated with rough and high-thermal inertia bedrock outcrops. In addition, away from the Seitah margin, regolith becomes dominated by strong CPX bands, including a strong broad band at 2 m that is not present in the Maaz bedrock (spectrum 5 in Figure 5a).

The fact that the 1.08-1.2 m band in Maaz bedrock is relatively weak suggests that a different mineral with a broad band >1.05 m may be contributing, such as Fe-bearing feldspar, Fe-bearing glass, Ca-rich CPX, or a mixture of these minerals (Figure 5b; Adams & Guillaud, 1978; Cloutis & Gaffey, 1991a,b; Klima et al., 2011; Horgan et al., 2014). The presence of this weaker band causes some rough areas near the landing site to exhibit either muted red colors (BD1300) in the mafic RGB combination map in Figure 1. Other areas show as green due to the strong downturn beyond 1.5 m that is also common in these spectra, resulting in elevated LCPINDEX2 values.

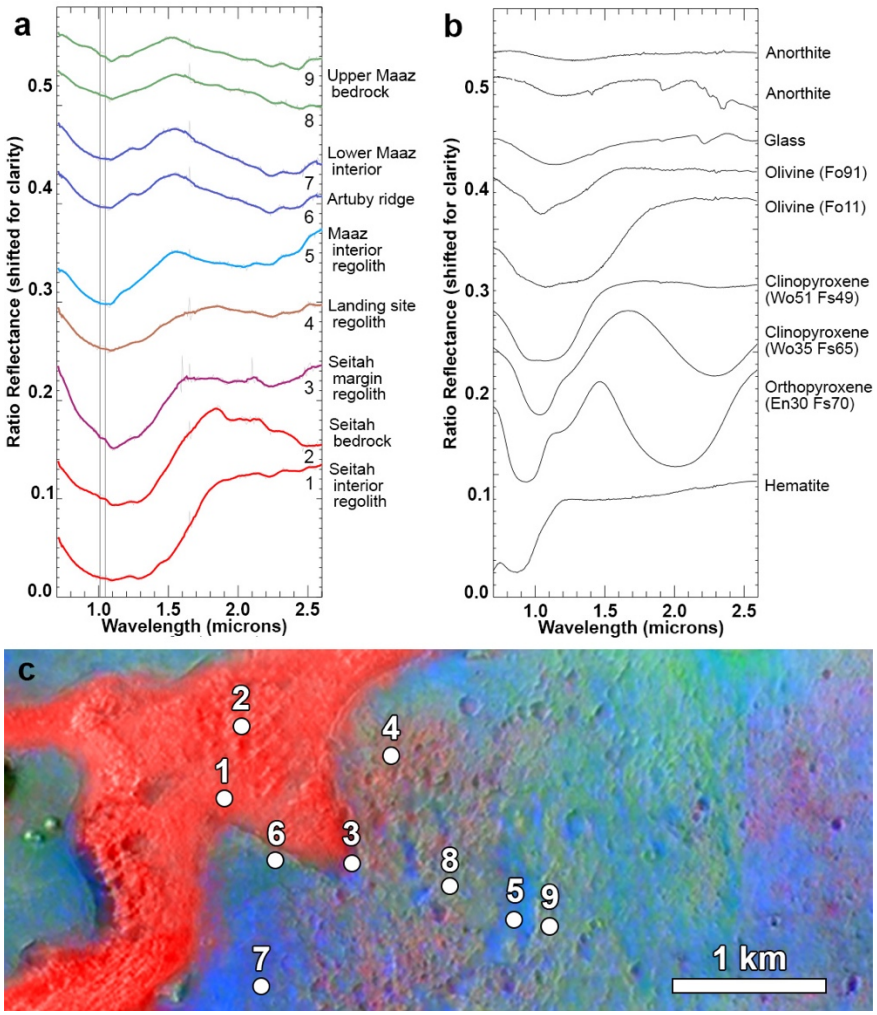

Figure 5: *(a) CRISM ratio spectra of the western crater floor, source image HRL000040FF. Vertical lines indicate the position of the join between the S- and L-detectors. Colors and numbers indicate color and location in RGB combination shown in (c). (b) Laboratory spectra of mafic minerals (Kokaly et al., 2017; Klima et al., 2011).*

4.2 Mastcam-Z

Outcrops of the Maaz formation show spectral variations in Mastcam-Z images that correlate well with morphologic facies described above. In particular, we find a sharp spectral division for dark rock surfaces between Maaz formation members: Chal, Nataani, and Roubion member rocks typically exhibit strong red slopes between 445-750 nm and a sharp peak near 750 nm, while Rochette

and Artuby member rocks typically exhibit relatively flat spectra 600-1000 nm with peaks often shifted to below 700 nm (Figure 6a). Stronger absorptions at short wavelengths in Chal, Nataani, and Roubion are likely due to ferric iron in primary or secondary minerals, suggesting more oxidizing conditions during emplacement or later alteration compared to Rochette and Artuby.

Maaz formation rocks also often show a variety of broad absorption bands at longer wavelengths consistent with Fe-bearing minerals (Figure 6). Three types of absorption bands are the most common. (1) A narrow to broad V-shaped band centered near 860 nm, consistent with crystalline red hematite (Morris et al., 1985; Horgan et al., 2020b) and most common in Chal and Roubion. (2) A broad band centered between 900-950 nm, consistent with orthopyroxene or Ca-poor and Fe-rich clinopyroxene (e.g., ferrosilite or pigeonite; Cloutis & Gaffey, 1991a), or possibly some ferric minerals like nontronite or goethite (Townsend, 1987; Rudolph et al., 2022; Haber et al., 2022). This band is variably present in all members. (3) A broad band superposed on a blue slope toward the end of the wavelength range, potentially suggesting a very broad band with a center >1030 nm like in olivine, clinopyroxene, Fe-bearing glass, or feldspar (Horgan et al., 2014). Nataani exhibits the broadest and deepest >1000 nm absorption bands, with some occurrences in Roubion as well. In many cases, these absorption bands may combine to create a more complex shape (e.g., both hematite and pyroxene bands in Roubion, Fig. 6a).

Spectral parameters applied to Mastcam-Z images of Maaz formation abrasion targets in Figure 7 clearly demonstrate the spectral differences between the Maaz members. These images are color combinations of spectral parameters measuring slopes (via reflectance ratios) and band depths. In this "mafic" color combination, red is the ratio R0R/R1 (630 nm/800 nm), which is high for spectra with peaks shifted to short wavelengths, and here indicates relatively unoxidized surfaces dominated by ferrous silicates like olivine and CPX. Green is the band depth at R3 (910 nm) relative to R1 (800 nm) and R5 (978 nm), which is high for spectra with strong ~900 nm bands, including OPX, Ca-poor CPX, and ferric alteration minerals. Blue is the ratio R1/R5 (800 nm/978 nm), which is high for spectra with absorption bands centered at longer wavelengths like olivine, Ca-rich CPX, Fe-bearing glass, or feldspar. In this color combination, the Chal member rock Sid is dominated by green (Fig. 7a) and Roubion is green and magenta (Fig. 7b), while the Rochette member rock Rochette is red and magenta (Fig. 7c) and the Artuby member rock Rimplas is blue and magenta (Fig. 7d).

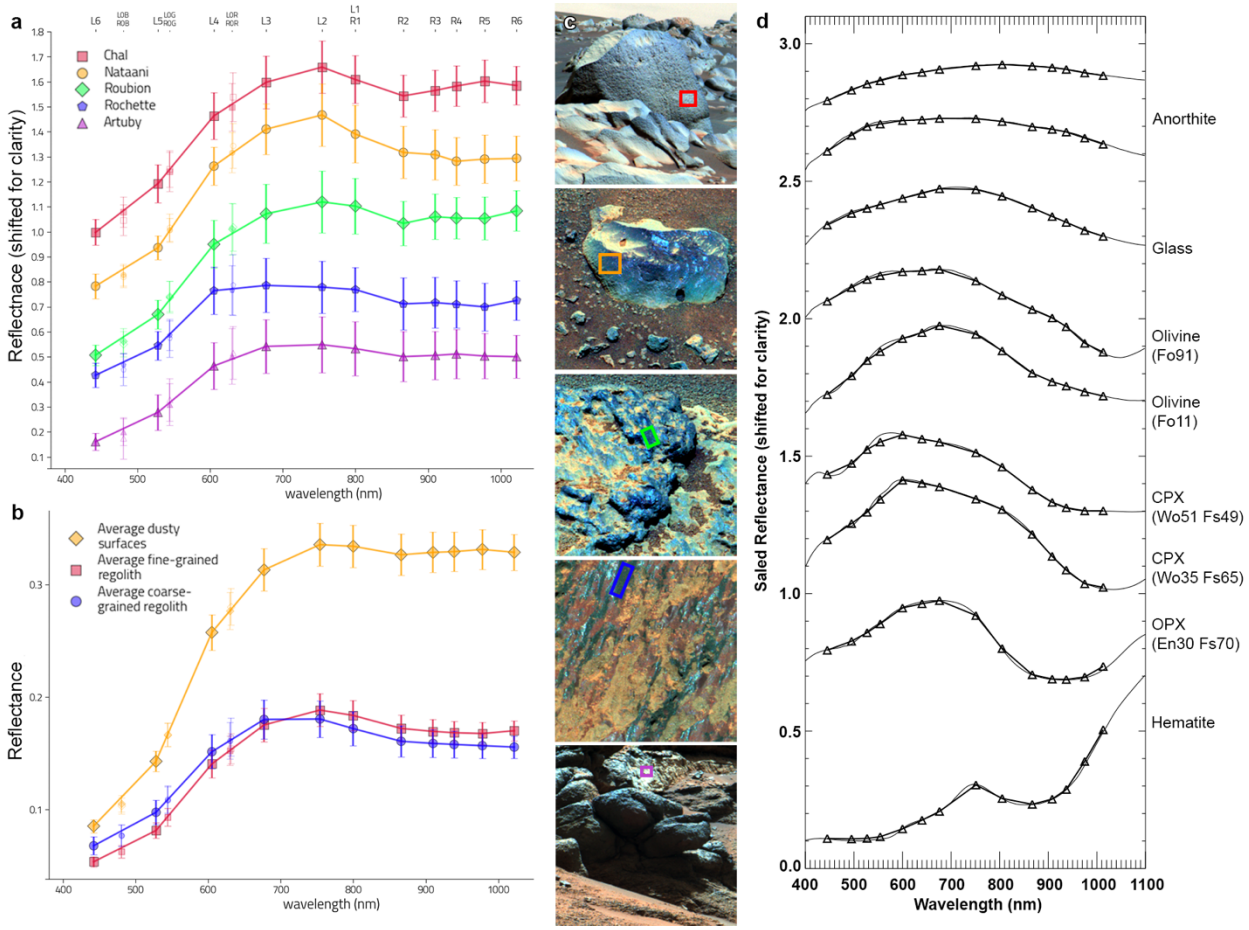

Figure 6: *Mastcam-Z multispectral data for Maaz formation members. (a) Representative spectra from dark, relatively uncoated surfaces, scaled at 600 nm and stacked for clarity. (b) Average spectra from fine- and coarse-grained regolith targets in the Maaz and Seitah formations and from average dusty surfaces (Vaughan et al., this issue). (c) Source images, top to bottom: Chal boulder, sol 372 zcam03330; Tseebii cobble, sol 112 zcam03161; Mont Brune outcrop, sol 145 zcam03186; Rochette block, sol 187 zcam03213; Artuby outcrop, sol 175 zcam03310. (d) Lab spectra in Figure 5 convolved with Mastcam-Z filter bandpasses.*

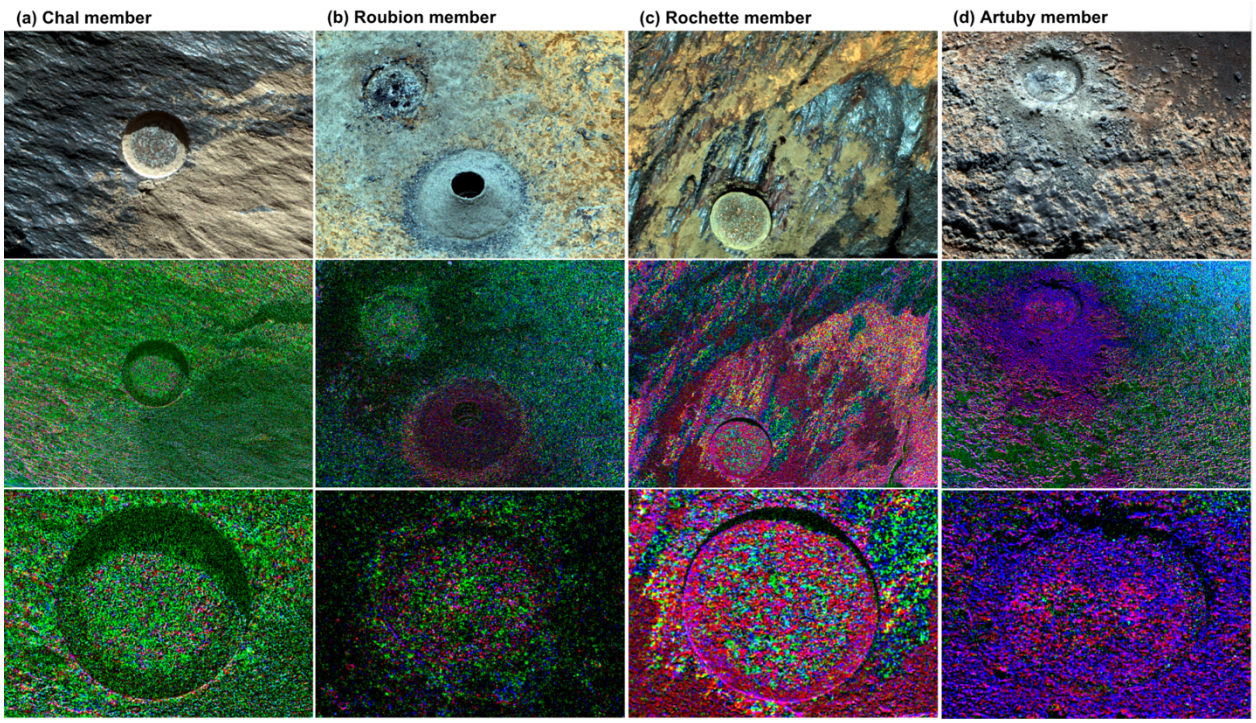

Figure 7: *Mastcam-Z images of Maaz fm. abrasion patches. (a) Alfalfa abrasion on the Sid block near the boundary of the Chal mb. (sol 368 zcam03328). (b) Guillaumes abrasion on the Roubion paver in the Roubion mb. (sol 166 zcam3200) (c) Bellegarde abrasion on the Rochette block in the Rochette mb. (sol 187 zcam03213). (d) Montpezat abrasion on the Rimplas outcrop in the Artuby mb. (sol 350 zcam03318). (top row) Enhanced color view from right Bayer images, (middle row) "mafic" red/green/blue spectral parameter combination as described in section 4.2 for the full scene and (bottom row) within the abrasion patches. All images are stretched as red (R0R/R1): 0.95-1.15, green (BD910): 0.02-0.1, blue (R1/R5): 1.04-1.15.*

We can investigate the petrologic origin of these natural surface spectral properties by using the abrasion patches created by Perseverance on four Maaz rocks from different members. These patches are created by percussive grinding of an area ~5 cm across to a depth of 4-8 mm (Moeller et al, 2020). This process removes surficial coatings and textures but not deeper weathering rinds. While most Maaz rocks show uniform surface color, all abrasion surfaces showed significant color variation at the sub-mm-scale that are resolvable by Mastcam-Z (Figure 8; 0.15-0.2 mm/pixel for the abrasion patches, making features ~0.5 mm resolvable). In higher resolution WATSON and RMI images (Figure 8), these color variations often correspond to coarse and angular primary grains, supporting an igneous interpretation for the Maaz formation that is also inferred from outcrop texture and mineralogy. (Farley et al., 2022; Wiens et al., 2022; Simon

et al., this issue; Udry et al., this issue; Alwmark et al., this issue).

Throughout the Maaz formation abrasion patches, hematite signatures are associated with visible red staining while pyroxene signatures are associated with gray grains, but the two signatures are often intimately mixed to produce complex absorption bands with intermediate properties. The Alfalfa abrasion patch in the Chal mb. exhibits red areas with strong hematite signatures and gray areas with weak broad pyroxene bands (Figure 8a), and the mixture of these two minerals appears to produce very broad bands with centers near 860 nm on the natural surfaces and tailings.

Alfalfa also exhibits large white feldspar crystal laths that exhibit minimal absorption <600 nm suggesting little ferric iron, and either flat slopes >600 nm consistent with typical (Fe-poor) feldspars or blue slopes suggesting the presence of ferrous iron, most likely due to sub-pixel mixing with pyroxene and/or Fe^{2+} substitution in anorthite (blue and cyan spectra, Figure 8a; Adams & Guillaud, 1978). Similar spectra are present in Bellegarde and Montpezat, associated with light gray areas (blue spectra, Figure 8c-d).

Hematite signatures are strongest in Chal but appear to weaken downsection in the Maaz formation. The Bellegarde abrasion patch in the Rochette mb. shows a clear mixing trend between moderate hematite signatures and pyroxene, in which red areas with weak hematite bands gradually shift their centers to closer to 900 nm and then >900 nm as the density of black to gray grains increases (Figure 8c). These weak pyroxene signatures also appear to dominate the natural surface and tailings spectra, which are notably not oxidized compared to Sid. Hematite bands are nearly absent in the Montpezat abrasion patch in the Artuby mb., which shows no strong pyroxene signatures but does show some spectra with slopes to long wavelengths that could suggest mafic minerals (green and cyan spectra, Figure 8d).

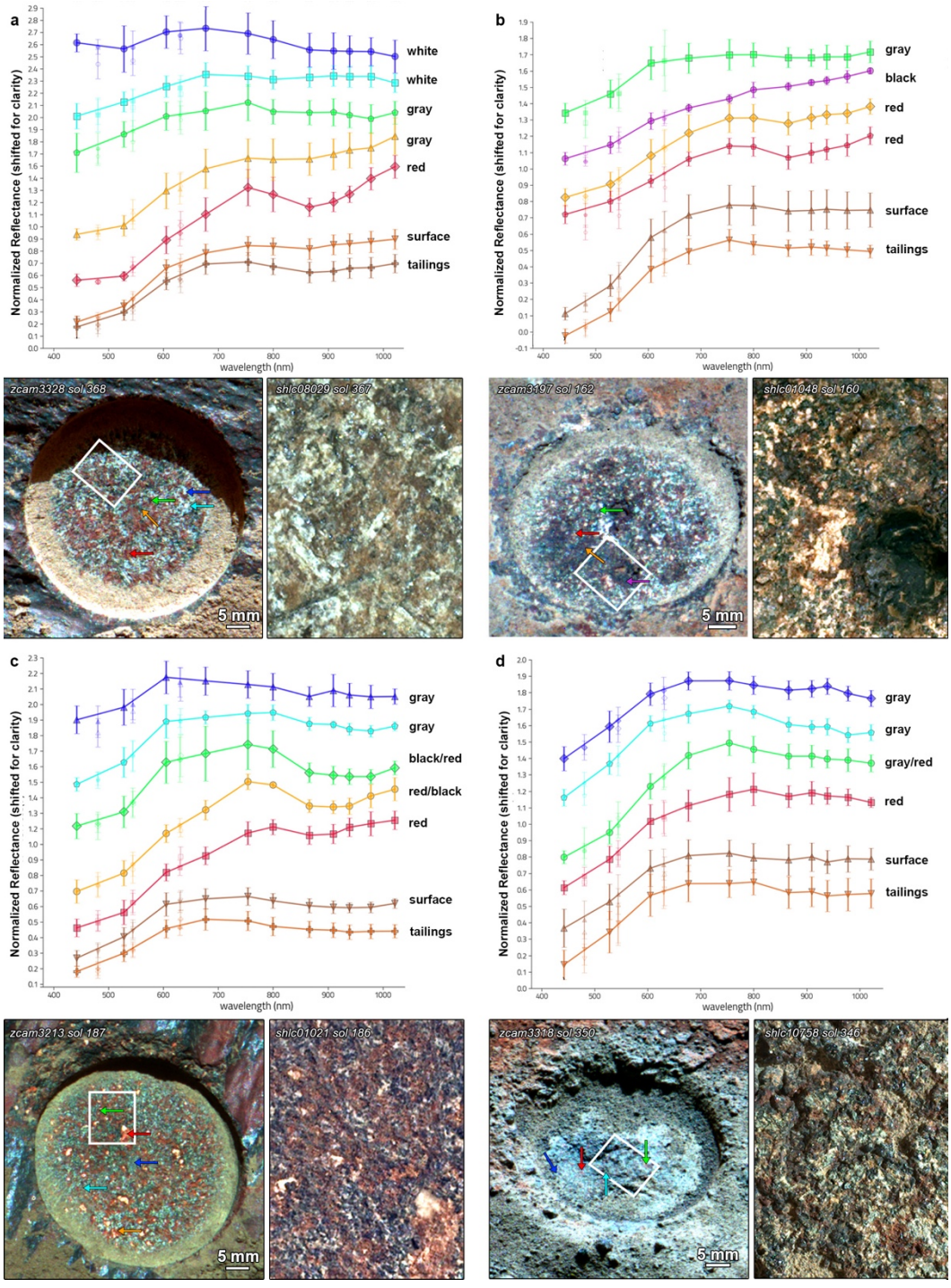
a
Normalized Reflectance (shifted for clarity)
wavelength (nm)
white
white
gray
gray
red
surface
tailings
zcam3328 sol 368
5 mm
shlc08029 sol 367
b
Normalized Reflectance (shifted for clarity)
wavelength (nm)
gray
black
red
red
surface
tailings
zcam3197 sol 162
5 mm
shlc01048 sol 160
c
Normalized Reflectance (shifted for clarity)
wavelength (nm)
gray
gray
black/red
red/black
red
surface
tailings
zcam3213 sol 187
5 mm
shlc01021 sol 186
d
Normalized Reflectance (shifted for clarity)
wavelength (nm)
gray
gray
gray/red
red
surface
tailings
zcam3318 sol 350
5 mm
shlc10758 sol 346

Figure 8: *Mastcam-Z spectra of Maaz fm. abraded patches compared to natural surfaces and borehole tailings, with L256 enhanced color image showing locations of spectra, where arrow colors correspond to spectra colors. White box indicates location of SHERLOC/WATSON image at right showing igneous textures in the abrasion patches. (a) Alfalfa abrasion on the Sid boulder in the Chal member, (b) Guillaumes abrasion on the Roubion paver in the Roubion member, (c) Bellegarde abrasion on the Rochette block in the Rochette member, (d) Montpezat abrasion on the Rimplas outcrop in the Artuby member.*

The Guillaumes abrasion patch on Roubion shows evidence for alteration in addition to oxidation. Guillaumes exhibits moderate hematite signatures in dark brown to red regions that are consistent with the overall trend downsection (orange and red spectra, Figure 8b), but these are mixed with black areas that exhibit very strong red spectral slopes and no discernible absorption bands (purple spectrum, Figure 8b). These strong red slopes could be consistent with opaque minerals like Mn-oxides and sulfides, or with some mixed-valence Fe-bearing phyllosilicates like greenalite. The black areas are found throughout the abrasion patch but are concentrated within and near surficial pits, suggesting a weathering rind.

A weathering rind at Roubion is further supported by the spectral differences between the abrasion and borehole tailings. In Figure 7b, the abrasion patch is largely green in the "mafic" parameter combination, and the abrasion tailings are black, suggesting low spectral contrast. However, the borehole tailings are magenta, consistent with much stronger spectral slopes. Dark surfaces on boulders in the area that are inferred to be Roubion based on morphology also show a magenta color in this parameter combination. This suggests that the coring process, which typically extracts material from up to 6-8 cm deep (Moeller et al, 2020), penetrated well through the weathering rind.

4.3 SuperCam VISIR

SuperCam VISIR spectra are highly complementary to Mastcam-Z multispectral data. While Mastcam-Z provides wide coverage, outcrop-scale context for VNIR spectral signatures, and direct connection of spectral signatures to specific grains in the abraded patches, SuperCam expands our wavelength range out to longer wavelengths 1300-2500 nm. This range can detect the far side of wide 1000 nm mafic mineral absorptions due to minerals like olivine, the ~2000 nm iron band in most pyroxenes, and narrow absorptions between 1900-2500 nm due to alteration minerals.

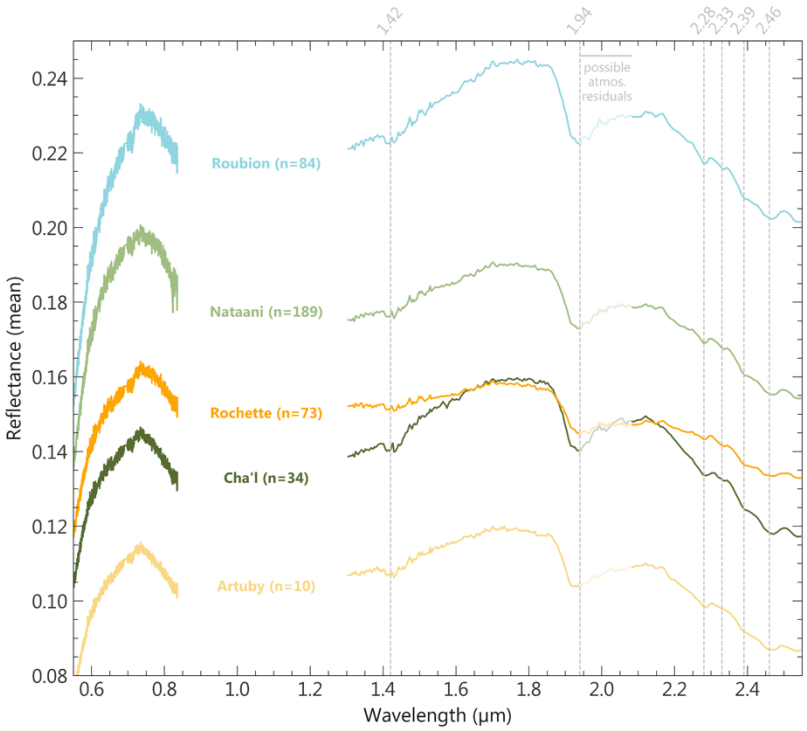

Figure 9: *Average SuperCam VISIR spectra from Maaz members (Mandon et al., this issue), including both dusty and LIBS-cleared natural surfaces and abrasion patches (n: number of individual point spectra averaged). Vertical lines indicate the position of narrow absorption bands associated with alteration minerals.*

Figure 9 shows average SuperCam VISIR spectra for Maaz formation members (Mandon et al., this issue). The members display overall similar spectral shapes, dominated by a broad band between 700-1700 nm consistent with olivine, feldspar mixtures, Ca-rich CPX, and some mixed valence Fe-bearing phyllosilicates. This band is strongest in Chal/Nataani/Roubion (~10-14% inferred band depth at 1100 nm) and weakest in Rochette/Artuby (~6-8%), consistent with the strength of the short wavelength side of this band in Mastcam-Z spectra of these members (Figure 6a). None of the average spectra show clear 2000 nm pyroxene bands, but independent components analysis (ICA) of the abraded patches indicates the presence of a strong broad band near 2300 nm consistent with CPX (Mandon et al., this issue). The average spectra also exhibit strong bands due to hydration at 1400 and 1900 nm, as well as weak variable bands between 2200-2500 nm due to alteration minerals, including phyllosilicates and sulfates.

4.4 SuperCam LIBS

Elemental chemistry from SuperCam LIBS of natural surfaces shows that the Chal and Nataani members are chemically distinct from the Rochette and Artuby members (Figure 10; Wiens et al., 2022; Udry et al., this issue). Chal and Nataani member averages are similar, and show higher SiO_2 than Rochette/Artuby (~52 vs. ~46wt.%). Roubion falls in the middle of the two groups for SiO_2 (~49 wt.%). The Maaz members also show similar abundances for other cations, except that the Artuby member shows higher MgO, CaO, and TiO_2 and slightly lower alkalis than the rest of Maaz. These calculations support early results from SuperCam that suggested that the Maaz fm. shows an overall increase in both silica and alkalis upsection (Wiens et al., 2022). The Content member, which is a texturally distinct and olivine-poor unit found within the Seitah formation, is most similar to Chal in these plots (although slightly more enriched in Al_2O_3, 12 wt.%) potentially supporting a similar igneous origin (Wiens et al. 2022; Brown et al., this issue; Udry et al., this issue).

In some cases, LIBS measurements exhibit compositions consistent with a single mineral, and thus can be used to assess the coarser-grained (>~300–500 m) component of the rocks. Udry et al. (this issue) detected 20 pyroxene grains in the Maaz fm. using this method, where the pyroxenes form a trend from augite ($Wo_{30–50}En_{10–22}Fs_{29–55}$) to a ferrosilite-like Fe-rich low-Ca pyroxene ($Wo_{3–9}En_{4–18}Fs_{73–93}$). No other primary minerals were detected, suggesting that high- and low-Ca CPX (augite and pigeonite) dominate the coarsest grains. Mineral assemblages derived from CIPW normative modal abundances show that feldspar is also abundant, where equal proportions (~40% each) of pyroxene and feldspar were modeled in upper Maaz members, compared to twice as much pyroxene as feldspar in lower Maaz members (~60% and ~30% respectively), with the remainder corresponding to quartz and minor phases, and no olivine modeled in either group (Udry et al., this issue).

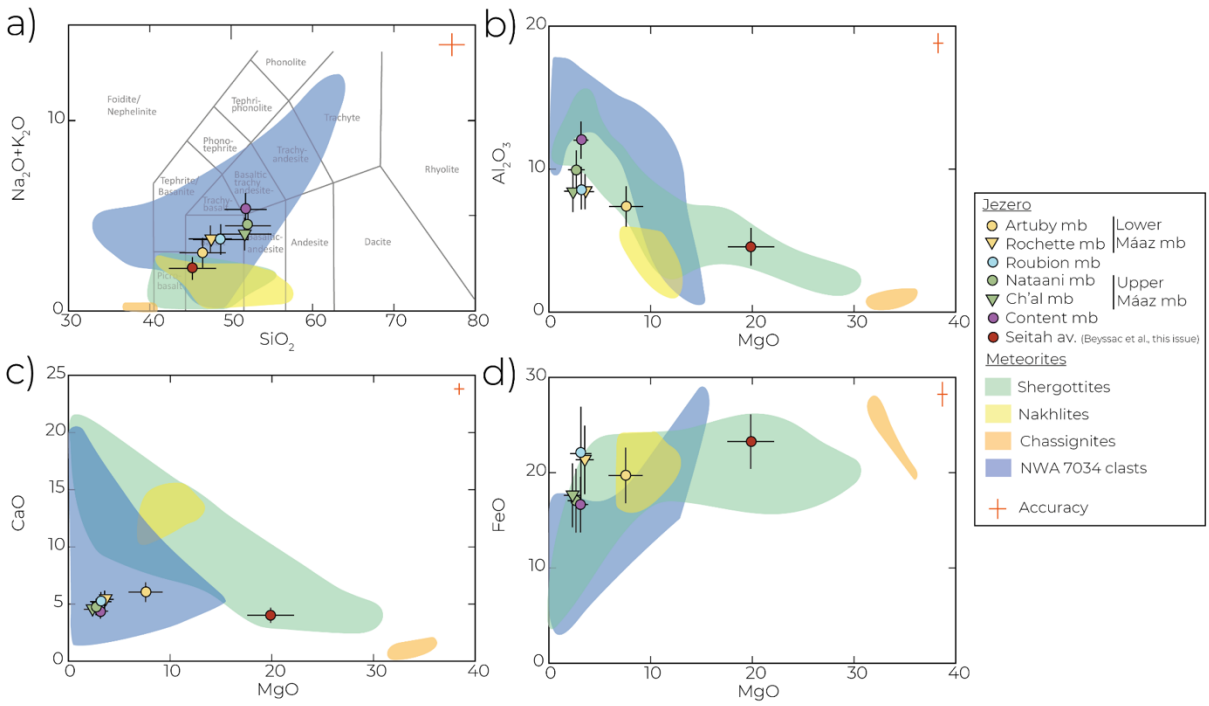

Figure 10: *SuperCam LIBS averages of major cations for natural uncoated rock surfaces in all crater floor members (Udry et al., this volume), compared to compositional fields for Mars meteorites (Udry et al., 2020).*

4.5 Origin of Maaz formation spectral signatures

Based on in situ chemistry and spectral data, the mineralogy of the Maaz formation is dominated by a mixture of feldspar with Ca-poor and Ca-rich pyroxenes, both relatively or very enriched in iron, with small quantities of hematite, phyllosilicates, sulfates, and other accessory minerals. Pyroxene would be expected to dominate reflectance spectra of the Maaz formation 1000-2500 nm. The Ca-poor pyroxene endmember identified by LIBS would be expected to exhibit absorption bands near 940 and 2100 nm (e.g., OPX or Wo35 CPX in Figure 5b; Klima et al., 2011), and the former is consistent with bands in Mastcam-Z spectra in the Maaz formation and the main spectral signature of the fine regolith. The Ca-rich pyroxene endmember (augite) typically exhibits absorption bands near 1020 and 2300 nm, where the latter is consistent with ICA analysis of SuperCam abrasion patch spectra in the Maaz formation and both are similar to CRISM observations of regolith-dominated terrains south of Artuby ridge.

However, CRISM and SuperCam VISIR spectra of upper Maaz bedrock are dominated by a single broad band between 0.7-1.5 m, centered between 1.08-1.2 m, and the short wavelength side of this band is commonly observed in

Nataani rocks by Mastcam-Z. In situ data clearly shows that this broad band is not due to olivine, as significant amount of olivine is not directly detected or inferred in the Maaz formation. Glass is also not expected to be a significant component of the coarsely crystalline lavas in the Maaz formation. It is common for pyroxene-dominated lavas to exhibit only the 1000 nm pyroxene band, as the weaker 2000 nm band can be obscured by opaque oxide minerals or other optical effects that lower overall spectral contrast (Carli and Sgavetti, 2011; Carli et al., 2015; Scudder et al., 2021). However, this explanation cannot explain the breadth of the band. Mixed valence Fe-bearing phyllosilicates often exhibit a broad and asymmetric band centered near 1.1 m that has been identified in deep weathering profiles on Mars (e.g., Bishop et al., 2013), and SuperCam VISIR spectra do detect weak Fe/Mg-OH bands near 2.3 m that are consistent with low abundances of a phyllosilicate mixture (Mandon et al., this issue). While we cannot rule out a contribution from phyllosilicates, these alteration bands are weak compared to the broad 1.1 m band and we do not observe them from orbit (Horgan et al., 2020a), suggesting that the 1.1 m band is too strong to be explained by this type of minor alteration.

The broad ~1.1 m band also resembles the broad and complex band exhibited by some Ca-saturated and Fe-rich pyroxenes (e.g., Wo51 Fs49 CPX in Figure 5b; Cloutis & Gaffey, 1991a; Schade et al., 2004; Klima et al., 2011; Horgan et al., 2014). This spectral type of pyroxene ("Type A") occurs when other cations prevent Fe^{2+} from occupying both possible octahedral cation sites, and thus tends to correlate with high abundances of Ca^{2+} (>~Wo45). The broad band is modeled as a triplet of bands around ~0.94, ~1.03, and 1.15 m, with variable depths that lead to complex and variable spectral shapes (Schade et al., 2004). While the Maaz formation does appear to contain significant Ca-rich pyroxenes, it is unclear whether or not these are Ca-saturated.

Finally, the ~1.1 m band could be due to coarse Fe-bearing feldspar crystals, or a mixture of coarse feldspar with pyroxene. Pure feldspars do not exhibit diagnostic absorption bands at visible/near-infrared wavelengths, but substitution of even small amounts of Fe^{2+} results in a broad and shallow band centered between 1.1-1.3 m, and most plagioclases more sodic than An50 contain sufficient iron to exhibit this band (Adams & Goullaud, 1978). This band is not usually apparent in igneous rocks, as plagioclase is relatively transparent compared to mafic minerals, and thus even >5-25% olivine or pyroxene is sufficient to obscure this band (Serventi et al., 2013; Cheek & Pieters, 2014). However, laboratory studies have shown that mixtures of coarse plagioclase grains and Type A pyroxene are still dominated by plagioclase even in a 1:1 mixture (Rogers & Nekvasil, 2015), perhaps due to both the relatively low spectral contrast in this spectral type of pyroxene and the large grain size of the plagioclase. This may be similar to upper Maaz members, which have a ~1:1 mixtures of plagioclase and pyroxene and exhibit coarse plagioclase crystal laths in the Alfalfa abrasion patch (Figure 8a).

Thus, we hypothesize that the visible/near-infrared spectral signature of upper

Maaz rocks is due to a combination of coarse plagioclase and Ca-saturated pyroxene, with a small amount of low-Ca pyroxene. CRISM spectra of upper Maaz also show a weak band near 860 nm consistent with hematite, which is consistent with Mastcam-Z spectra of the natural surfaces of Chal and Nataani (and to a lesser degree, Roubion) that are dominated by hematite mixed with some pyroxene (green in Figure 7).

CRISM spectra of lower Maaz areas (dark blue spectra in Figure 5a) have some qualities that resemble upper Maaz, including a broad band between 700-1700 nm and a strong downturn at longer wavelengths. However, the broad band is centered at shorter wavelengths than upper Maaz, closer to 1000 nm, and the lower Maaz CRISM spectra also show an additional upturn near 2500 nm that we attribute to the long edge of the CPX ~2000 nm band, which is not observed in any of the average SuperCam bedrock spectra. Instead, SuperCam and CRISM spectra of fine regolith on the crater floor show broad absorptions centered near 1000 and 2100 nm consistent with CPX (Mandon et al., this issue), suggesting that regolith is contributing to the CRISM signature (Mandon et al., this issue; Vaughan et al., this issue). Thus, we hypothesize that the lower Maaz spectrum is a mixture of upper Maaz-like bedrock (green spectra in Figure 5a) and Maaz regolith (light blue spectrum in Figure 5a).

The Maaz formation may be a source for at least some of the local fine regolith (Vaughan et al., this issue). Mastcam-Z spectra of fine-grained regolith exhibit a broad band centered >900 nm consistent with CPX, and similar weak bands are found in Mastcam-Z spectra of abraded patches throughout the Maaz formation. However, this band most strongly dominates the natural surface of the Rochette member (red/magenta in Figure 7). SuperCam also reported the highest average CaO abundances at Artuby ridge (Rochette and Artuby members), which Wiens et al. (2022) attributed to higher CPX abundances. This suggests that Rochette and the compositionally similar but more friable Artuby member is a possible local source of CPX-dominated fine regolith, and this hypothesis is supported by CRISM observations of concentrations of this signature around the Rochette fractured block surface morphology.

5. Stratigraphy

The stratigraphy of the Maaz formation could be locally variable, but the Artuby/Rochette members appear to be stratigraphically lowest, as they directly overlie the Seitah formation where it is exposed at the base of the Artuby ridge (Figure 4f). Nataani/Chal appear to be the stratigraphically highest members, as they occupy the highest elevations in the area. If this is the case, then the observation that Nataani/Chal are not present on top of or to the south of Artuby ridge suggests that they have been eroded from or were never deposited in this area.

However, the relationship between the Nataani/Chal and Artuby/Rochette

members is not well understood, as no unambiguous contact between Nataani/Chal and Rochette/Artuby rocks was identified close to the traverse. In addition, the Roubion member appears to underlie the Nataani member in the region of Polygon Valley (section 3.2), but its distribution outside of this area is unclear, so the relationship between the Roubion and Artuby/Rochette members is also unknown. While Perseverance passed by several key outcrops that could help constrain the stratigraphy, their distance makes morphologic interpretations more challenging and ambiguous. Here we use multispectral landscape views to help inform stratigraphic interpretations of distant outcrops, and integrate RIMFAX subsurface soundings to build local stratigraphic models.

5.1 Mastcam-Z multispectral landscape views

As with the abrasion patches, we find that the "mafic" parameter color combination described in section 4.2 (Figure 7) is helpful for discriminating between Maaz members in landscape and outcrop. Chal and Nataani both appear as green and the Roubion mb. shows up as magenta. The most resistant layers in the Rochette mb. are distinctly red, while more recessive underlying layers are more magenta, and Artuby shows small-scale mixing between magenta and blue. These multispectral parameters are helpful for assisting in member identification, but are most appropriate when used in parallel with morphologic assessments, as they are subject to modification by factors like dust, coatings, and variable illumination geometries. Dusty and purple coated surfaces look weakly green because they have very low values for the slope parameters in the red and blue channels and weak BD910 values in the green channel. However, a continuous green color correlated with dark rock surfaces is likely due to rock properties.

To develop a more comprehensive stratigraphy, we focus on the landing site, where Nataani and Chal are clearly present. If they are stratigraphically higher than Rochette/Artuby, we may expect these units to be present in the area at lower elevations. And indeed, a Rochette-like resistant and blocky cap forms the margin of the Maaz Fm. to the west of the landing site (Figure 11a). While this outcrop was not visited by the rover, the cap rock appears bright red in our Mastcam-Z "mafic" parameter combination, consistent with Rochette, and shows Rochette-like spectra, suggesting that this is the northern equivalent of Rochette.

To the south of this outcrop, the Rochette-like margin is overlain by rough, pitted, dark, and layered blocks similar to Roubion, with a magenta color in the mafic RGB consistent with Roubion (Figure 11b). Above this area, a higher ridge exhibits massive layers. These layers are at elevations consistent with Nataani, with the green color in the mafic RGB expected for Nataani. The terrain to the east of these outcrops is dominated by the Nataani mb., which transitions to the Chal member further east. This suggests a relatively simple stratigraphy near the landing site of Rochette overlain by Roubion, Nataani, and

then Chal (Figure 12a). Outcrops consistent with Artuby were not apparent in rover views of this area.

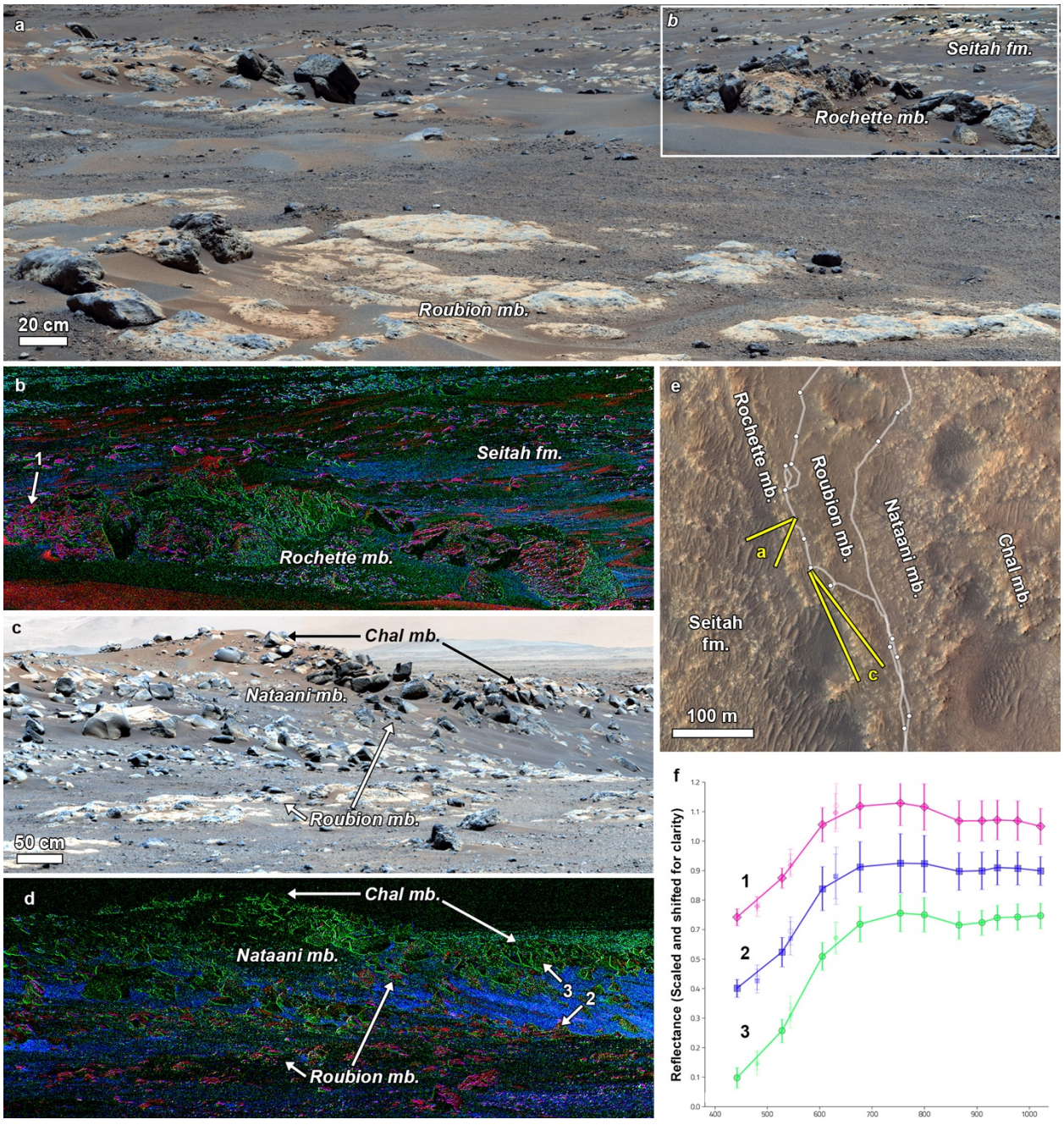

Figure 11: *Outcrops at the margin of the Maaz fm. west of the landing*

site. (a) Dark and pitted paver forming rocks consistent with the Roubion member transition to massive pitted blocks consistent with the Rochette member at the western edge scarp of the Maaz fm., overlooking Seitah (sol 124 zcam08121). (b) Multispectral mafic parameter combination similar to Figure 7, where magenta/red corresponds to additional reflectance near 650 nm typical of Rochette and Roubion member rocks (spectrum from point 1 shown in f; sol 124 zcam03170). (c) The Roubion plateau is overlain by Nataani and Chal member outcrops on the margin of a small impact crater cut into the Maaz western scarp (sol 129 zcam03173), where morphological interpretations are supported by (d) the mafic parameter combination. (e) Context map showing approximate viewsheds for a-d. (f) Plot of spectra from locations numbered in b/d.

5.2 RIMFAX subsurface soundings

RIMFAX subsurface soundings support this overall interpretation of the stratigraphy near the landing site (Figure 12a). Near the western margin of Maaz and the outcrops in Figure 11, the Maaz formation appears to be 3-4 m thick, overlying the Seitah fm. Within this section, at least three distinct radar units can be identified above the Seitah fm. The lowermost unit is ~2 m thick and shows strong blocky reflectors at its top surface, consistent with the radar profile of the Rochette member on Artuby ridge (Figure 12a) and supporting the interpretation of Rochette outcropping along the margin in Figure 11a. The middle unit is a radar relatively "transparent" zone ~1 m thick, likely indicating low density and/or fine grained material. This unit is overlain by a subtly layered top unit, 1-2 m thick. Based on nearby outcrops, one interpretation is that the middle unit is the Roubion member and the top unit is Nataani, likely with some regolith cover. However, given how close Roubion is to the surface in this area and that it tends to exhibit rough layering at smaller scales than Nataani, it is also possible that Rochette is overlain by a localized low density sedimentary unit, and that the top unit is Roubion.

Moving south into Polygon Valley (Figure 12b), RIMFAX data show that the surficial Roubion member appears to be directly overlying dipping beds of the Seitah fm., at about 1 m depth. Rochette and Artuby members are not present, suggesting that they were either never present in this location or that they were eroded prior to the emplacement of Roubion. Given that this area appears to be a zone of erosion, we favor the latter interpretation. Indeed, a U-shaped radar transparent zone is present below Roubion in the center of Polygon Valley, potentially due to a sediment-filled erosional trough that pre-dated emplacement of Roubion, supporting this hypothesis. Thus, the only place where the Artuby member is clearly present around the southern or eastern margin of Seitah is along Artuby ridge (Figure 12c), perhaps suggesting a different emplacement and/or erosion history compared to the Rochette member.

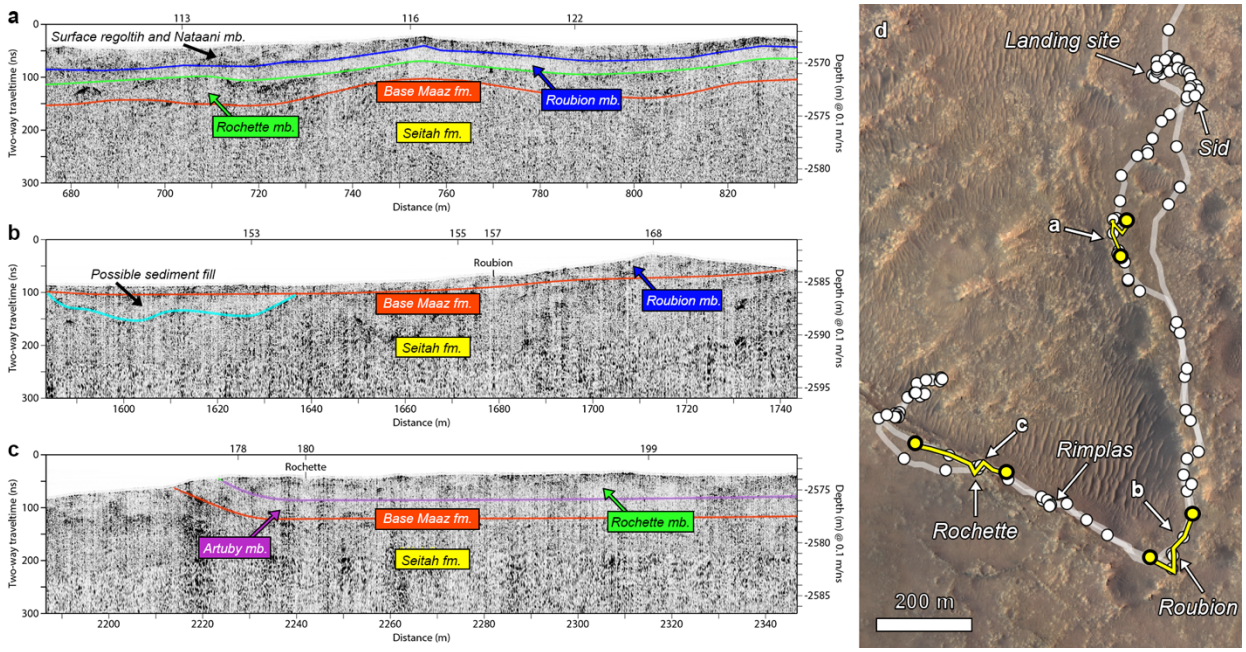

Figure 12: *RIMFAX profiles along key stratigraphic intervals in the Maaz formation. (a) Subsurface reflections near the western margin (sols 112-123) show several distinct units, including a unit with strong upper surface reflections that we interpret as the Rochette mb. and a transparent unit that we interpret as Roubion mb. The Artuby mb. is not apparent in this area. Note the double-back of the route, centered on sol 116, resulting in similar sections to the left and right of 116 label in the radargram. (b) Polygon Valley (sols 152-169) shows a thin (~1 meter) layer of Maaz fm. rocks that correspond to weathered Roubion mb. at the surface, overlying dipping beds of the Seitah fm. Rochette and Artuby are not apparent in this area. (c) The rover traverse up to and along Artuby ridge (sols 177-200) shows that the Maaz fm. (Artuby and Rochette mbs.) dips away from the Seitah fm. near the margin. The layers flatten out after sol 180 where the rover took a 90 degree turn to drive along the ridge. (d) Context map showing locations of drive segments in a-c.*

5.3 Stratigraphic models

Thus, the outcrop properties of the Maaz formation appear to be consistent with a stratigraphic sequence from top to bottom of Chal, Nataani, Roubion, Rochette, Artuby members, all overlying the Seitah formation. However, the dips and strikes of the members and their variability is not well constrained from this analysis and requires further detailed study with RIMFAX soundings. In addition, the different members have distinct distributions, as the Artuby mb. is not detected outside of Artuby ridge. The Rochette mb. is not detected in the area of Polygon Valley, suggesting that if it was once continuous, that it must

have undergone significant erosion prior to the emplacement of the Roubion member. Interestingly, the Roubion mb. is underlain by lenses or layers of radar transparent zones at both the landing site and in Polygon Valley, possibly indicating sediments and supporting a period of erosion before it was emplaced.

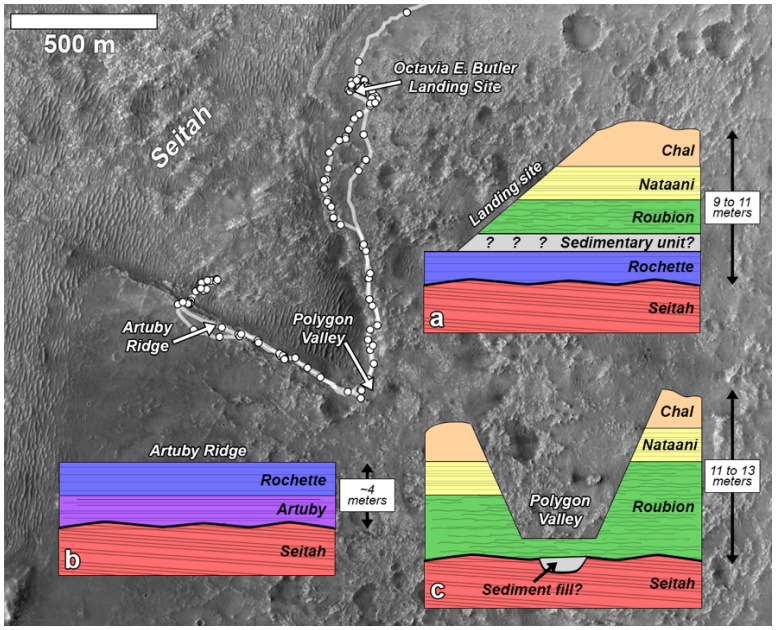

Figure 13: *Local stratigraphic models for the crater floor, based on relationships in outcrop and RIMFAX data, near (a) the landing site, (b) Artuby ridge, and (c) Polygon Valley (see section 3.2 for discussion of Roubion thickness). These models are simplifications of the stratigraphy and do not make predictions for local or regional dips.*

6. Discussion

6.1 Similarities and differences between Maaz formation members

Based on orbital and in situ morphology and spectral properties as well as in situ composition, we can broadly split the Maaz formation along the rover traverse into two distinct groups. This could be due to the presence of two distinct series of lava flows that may have different emplacement histories and timing. This interpretation is consistent with Wiens et al. (2022), who first proposed a similar split based on LIBS compositional differences.

"Lower" Maaz includes the Artuby and Rochette members, and is represented by the Montdenier and Montagnac samples from the Rochette member. Lower Maaz members exhibit similar mafic (basaltic) bulk chemistries, relatively un-

oxidized natural surfaces with weak CPX signatures in Mastcam-Z data, and outcrop expressions dominated by thin layers or planar joints. The two members do exhibit somewhat distinct morphological and spectral properties, so they may have experienced different emplacement or modification histories. In particular, while a lava flow origin is strongly supported for the Rochette member (Crumpler et al., this issue; Simon et al., this issue), a pyroclastic origin has not been ruled out for the Artuby member (Alwmark et al., this issue), but the chemical similarity to Rochette would be consistent with a similar volcanic source (Udry et al., this issue).

"Upper" Maaz includes the Chal and Nataani members, and is represented by the Hahoonih and Atsah samples from near the boundary between Chal and Nataani. Upper Maaz members exhibit similar bulk chemistries that are less primitive and more enriched in SiO_2 (basalt to basaltic andesite; Wiens et al., 2022; Udry et al., this issue) than lower Maaz, variable hematite, pyroxene, or mixed signatures on their natural surfaces in Mastcam-Z data, massive morphologies, and textures consistent with lava flows. The primary difference between Chal and Nataani appears to be the smooth top surface and thick layers of Nataani vs. the massive and boulder-producing morphology of Chal. These differences are consistent with variable lava flow morphologies, where Nataani may have been emplaced as layers of pahoehoe lobes, while Chal may have been one or more thick and blockier flows.

Roubion is stratigraphically intermediate between these groups and may be transitional. While its average bulk chemistry and dark pitted and layered textures are more similar to lower Maaz, Roubion has a distribution that is much more similar to upper Maaz, and shows surface oxidation more similar to upper Maaz.

The Content member of the Seitah formation is a pitted olivine-poor unit that drapes the Bastide ridge sampled by Perseverance in Seitah (Beysaac et al., this issue). Compositionally, the Content member is chemically similar to upper Maaz (and even a little more Al-enriched; Udry et al., this issue), and thus could be a related igneous unit. For example, given the draping nature of the Content mb., an origin as a late tephra deposit from the same source as upper Maaz is plausible.

6.2 Extent of Maaz formation members on the crater floor

From orbit (Figure 14), lower Maaz appears to be associated with relatively smooth regolith-dominated surfaces with fragmented blocks, and we hypothesize that these form due to the thinly layered and variable recessive nature of these members. These recessive properties likely lead to poor crater preservation in these areas. The CRISM CPX signatures that dominate these areas are likely due to regolith that we hypothesize is sourced from these members based on their similar spectral properties. The area southwest of Artuby ridge exhibits low thermal inertia values consistent with regolith cover (Figure 14d).

Several observations suggest that lower Maaz rocks extend beyond the area of the crater floor campaign. A distinct region toward the middle of the crater floor exhibits similar spectral, textural, and thermal inertia properties as lower Maaz, and could be a continuation of these members (Figure 14b). Furthermore, we hypothesize that because the more resistant layers in Lower Maaz (Rochette member) define the sharp margins of Maaz near Seitah, that they (or similar units) could be responsible for the lobate margins that characterize much of the crater floor more generally.

We hypothesize that lower Maaz members may also be the primary crater floor rocks underlying the delta. The Maaz formation near the delta is largely obscured by thick regolith, but exhibits lobate margins similar to Artuby ridge and a surface texture similar to that observed south of Artuby ridge. In some locations, this area exhibits orthopyroxene absorptions in CRISM data similar to the delta top, and thus consistent with erosion from the delta or previously overlying sediments (Alwmark et al., 2021). However, the overall spectral signature in the area is most consistent with a mixture of orthopyroxene and clinopyroxene, which could suggest that lower Maaz is the main substrate in the area.

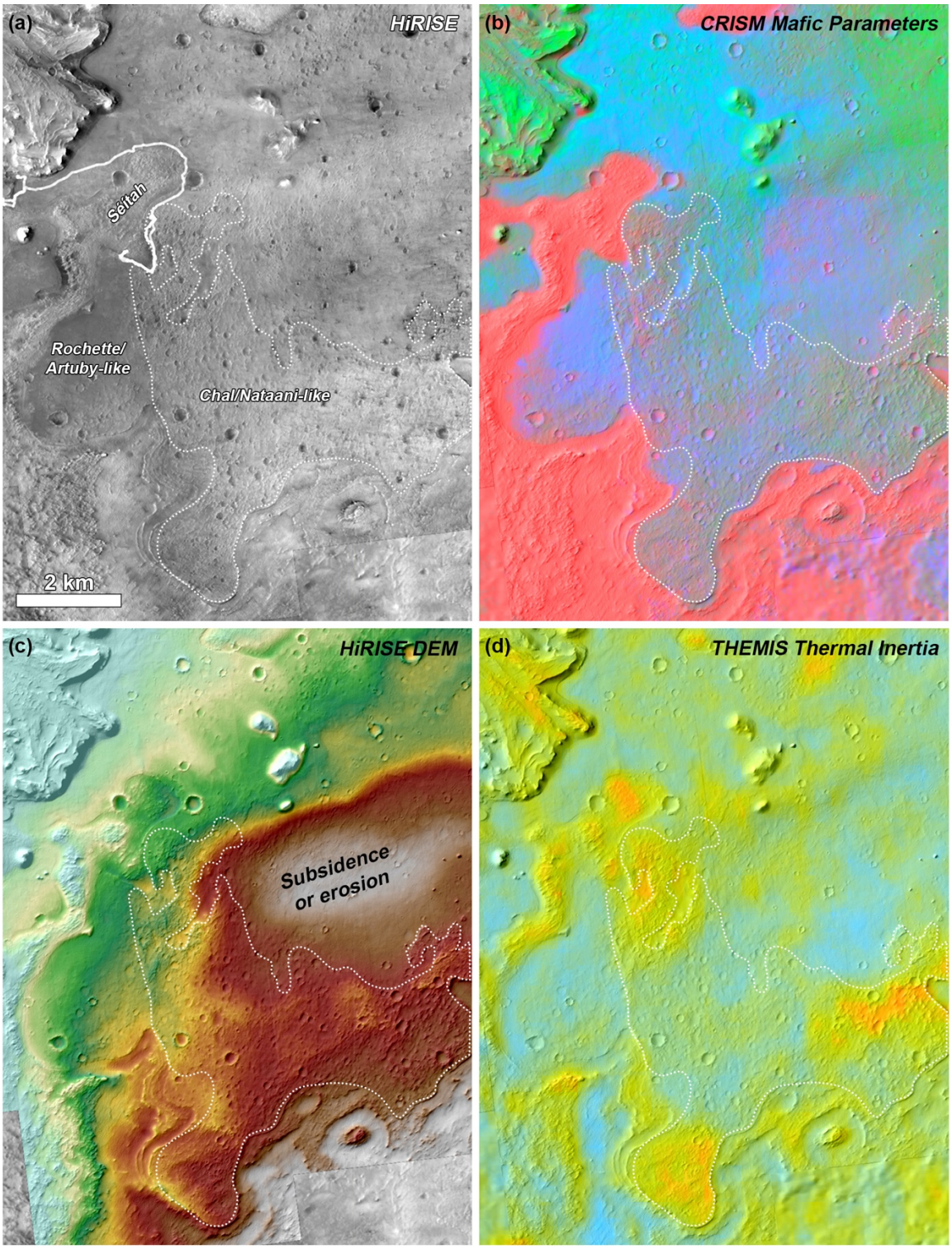
(a)
HiRISE
Séítah
Rochette/
Artuby-like
Chal/Nataani-like
2 km
(b)
CRISM Mafic Parameters
(c)
HiRISE DEM
Subsidence
or erosion
(d)
THEMIS Thermal Inertia

Figure 14: *Inferred extent of Chal/Nataani-like surfaces (dashed line) on the southwestern crater floor near the landing site, based on orbital datasets. (a) HiRISE mosaic, (b) CRISM mafic parameters color combination, (c) HiRISE elevation, (d) THEMIS thermal inertia, where (b-d) are all colorized shaded relief from HiRISE.*

While these interpretations suggest that lower Maaz is widespread across the crater floor, upper Maaz members may be more localized. Upper Maaz members are associated with rough textures and partially preserved craters, and we hypothesize that the CRISM signatures in the rough terrains to the east of the landing site are due to coarse feldspar and high-Ca pyroxene as observed most strongly in Chal/Nataani. These properties extend across an area south and southeast of the landing site (dashed outline in Figure 14). To the south of Artuby ridge, upper Maaz forms a sharp boundary that could represent an erosional front. However, there is no evidence for Chal or Nataani-like materials west of this margin in any orbital datasets, so we instead interpret this as a possible original flow margin. Furthermore, no textures or spectral properties consistent with upper Maaz are observed north or west of the landing site. Together, these properties are consistent with emplacement of Upper Maaz as lava flows that flowed across but did not fill the crater floor, where their extent was controlled by paleotopography at the time of emplacement.

6.3 Possible volcanic sources

Several possible volcanic edifices are present in and around Jezero that could have been sources for the Maaz formation lavas. Jezero Mons is a very large conical edifice rising 2 km above the SE rim of Jezero that is most likely volcanic in origin (Figure 15a; Horgan et al., 2020a). While Jezero Mons is currently downslope from the Maaz formation, further careful analysis of the paleotopography of the area is required to rule it out as a lava flow source, and any explosive eruptions at Jezero Mons would be expected to emplace tephra into Jezero crater (Ravanis et al., 2022). Similar but smaller steep-sided edifices are present to the southwest of Jezero (Figure 15e). Jezero Mons and these other edifices could represent a volcanic field, which would suggest significant regional volcanic activity in the past. Jezero crater itself contains a variety of mounds

that could be volcanic, but are largely interpreted as slumped crustal blocks from the Jezero impact (Figure 15d; Sun and Stack, 2020). The most anomalous of these is a ~200 meter high isolated edifice just inside the eroded northern rim of Jezero (Figure 15c). This northern edifice is the only volcano-like feature identified so far that is upslope from the Maaz formation and thus is currently the most plausible source, if it is a volcanic vent.

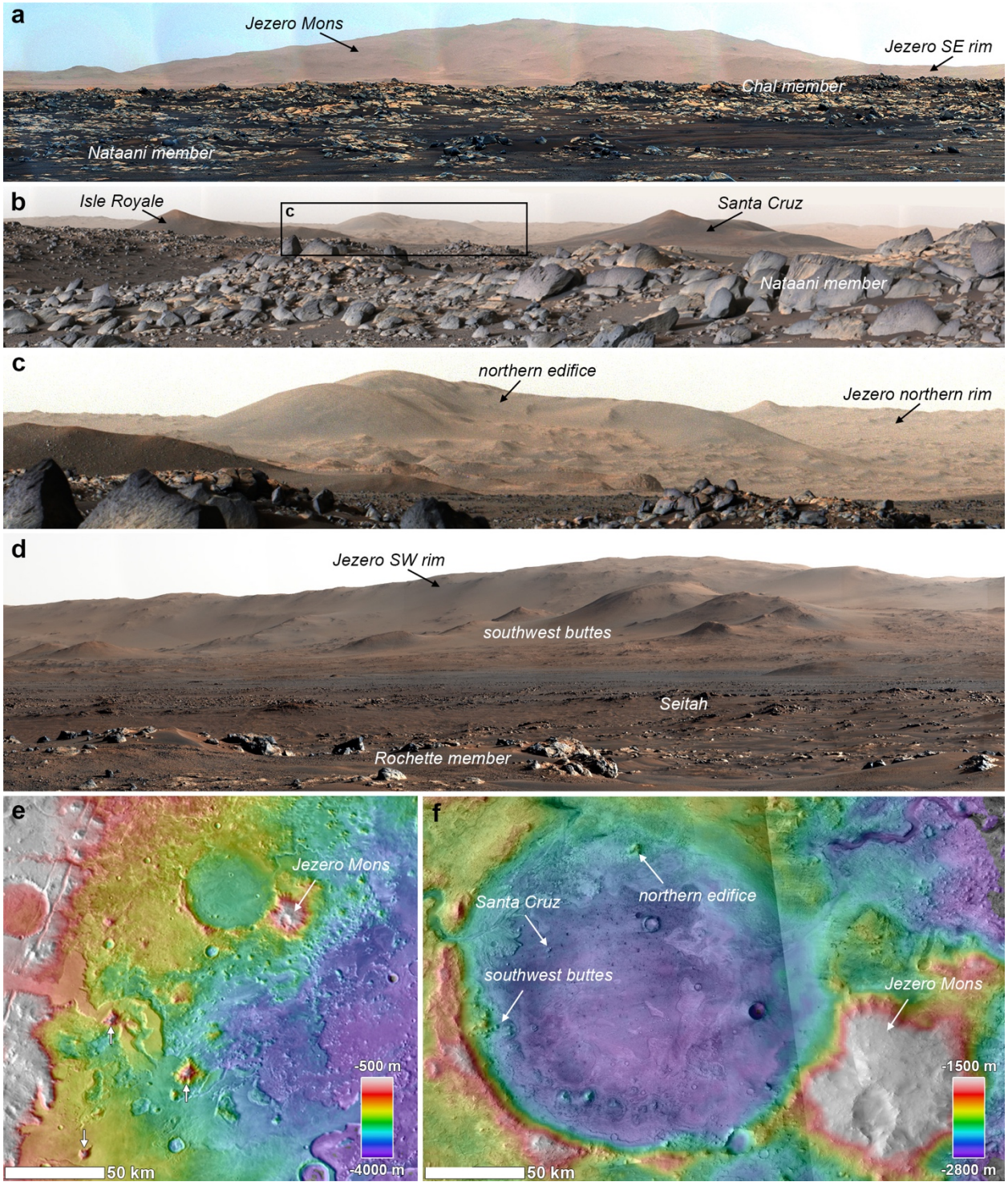
a
Jezero Mons
Jezero SE rim
Chal member
Nataani member
b
Isle Royale
c
Santa Cruz
Nataani member
c
northern edifice
Jezero northern rim
d
Jezero SW rim
southwest buttes
Seitah
Rochette member
e
Jezero Mons
-500 m
-4000 m
50 km
f
Santa Cruz
northern edifice
southwest buttes
Jezero Mons
-1500 m
-2800 m
50 km

Figure 15: *Mastcam-Z enhanced color views of possible volcanic features in and around Jezero crater. (a) Jezero Mons, approximately 40 km SE of the landing site and rising 2 km above the crater rim (sol 104, zcam08064). (b) Channel Islands buttes erosional sedimentary remnants, framing large edifice (~200 m high) inside northern rim, zoom shown in (c) (sol 353, zcam08382). (d) Southwest buttes interpreted as crustal blocks from the Jezero impact (sol 128, zcam08129). (e) Regional topographic context (blended MOLA/HRSC over THEMIS daytime infrared) showing Jezero Mons and smaller steep sided edifices to southwest, the largest of which with peak elevations above -500 m are indicated by arrows. (f) Jezero local topography showing Jezero Mons and features in a-d.*

6.4 Emplacement history of the Maaz formation

The stratigraphically lowest visible unit in Jezero is the Seitah formation, which is interpreted as an olivine cumulate emplaced as a thick lava flow, lava lake, or intrusion (Liu et al., 2022; Wiens et al., 2022; Farley et al., 2022). Orbital data shows that Seitah-like materials are present throughout the Jezero crater floor and, along with the Maaz fm, obscure all underlying units (Goudge et al., 2015; Horgan et al., 2020), so any origin must account for the high volumes necessary to fill the crater. Emplacement models that produce the coarse olivine grains observed in Seitah typically require melt depths of tens or up to one hundred meters, and should produce a stratigraphy of olivine-poor cumulates overlying the olivine-rich cumulates observed in Seitah (Liu et al., 2022). Early hypotheses for the relationship between Seitah and Maaz suggested that the Rochette and Artuby members could represent the upper portion (Artuby mb.) and surface flow (Rochette mb.) of this melt body (Farley et al., 2022; Wiens et al., 2022). In situ, the Artuby member does display some morphological similarities to Seitah, including variably massive vs. layered/recessive outcrops, with bedding at similar scales. However, this may not be supported by the details of the mineralogy of lower Maaz compared to Seitah, which suggest distinct magma sources (Udry et al., this volume). If Artuby and/or Rochette are not representative of the upper portion of the Seitah melt body, then the actual upper portion must have been largely removed by erosion.

Thus, following the emplacement of Seitah, we hypothesize that a period of erosion created significant topography on the crater floor, including the ridges that make up Seitah today. Deposition of the Maaz formation on this paleosurface began with emplacement of the Artuby and Rochette members widely on the crater floor, most likely as lava flows that embayed Seitah (Farley et al. 2022; Wiens et al., 2022). Given that the Artuby mb. is not apparent beneath the Rochette mb. near the landing site, it may have either had a different initial distribution or undergone erosion prior to the emplacement of the Rochette mb.

Evidence points to additional erosion of the crater floor after the emplacement of the Rochette mb. lavas. Lower Maaz members are absent beneath the Roubion mb. in Polygon Valley, so if they were once continuous, they were eroded from this area prior to emplacement of the overlying units. This suggests that Poly-

gon Valley has been a persistent site of erosion through time, perhaps related to the topography of Seitah and interactions with dominant winds. In support of a period of erosion at this time, Roubion appears to be underlain by radar transparent zones consistent with fine-grained sedimentary deposits both at the landing site and in Polygon Valley. These deposits were not observed in outcrop, so could be consistent with a variety of origins, including locally reworked materials, an aeolian deposit, or a fluvio-lacustrine deposit. The Roubion, Nataani, and Chal members were all emplaced as lava flows on this modified surface, once again embaying Seitah but also filling Polygon Valley.

The crater floor also shows evidence for other topographic modifications following emplacement of lower Maaz, under the assumption that these members started out as flat lava flows: (1) local tilting of lower Maaz along Artuby ridge to achieve local slopes ~12 degrees (Figure 12c), possibly due to uplift of Seitah by an unknown process (Hamran et al., 2022), (2) subsidence of Jezero basin fill creating an overall slope of ~2-3 degrees toward the center of the basin (Figure 14c); (3) rebound of Isidis and Jezero basins, potentially producing complex regional tectonics. The evolution of the basin likely continued after upper Maaz was emplaced as well, as these members also do not exhibit the constant topographic profile expected for a lava flow. However, some subsidence likely already occurred prior to upper Maaz, as one interpretation of the sharp margin on upper Maaz south of Polygon Valley is that these flows embayed shallow slopes of Artuby/Rochette toward the delta.

Following emplacement of the Maaz formation, one or more periods of fluvio-lacustrine activity in Jezero created the western delta and likely covered the crater floor in 40 meters or more of lake sediments, which are now preserved only in the rim of Hartwell crater to the northeast and within the Channel Islands buttes to the north of the landing site (Figure 15b; Quantin-Nataf et al., this issue). Some of the alteration observed within the Maaz formation could be related to this main period of lake activity, however, the presence of tens of meters of dense lake sediments may have prevented significant infiltration of lake waters into the Maaz formation.

After cessation of lake activity, the lake sediments were eroded from the crater floor from east to west, gradually exposing the crater floor to impacts and producing a strong gradient in crater density increasing away from the delta (Quantin-Nataf et al., this issue). Additional weathering, erosion, and coating formation (Garczynski et al., this issue) shaped the crater floor that we observe today.

The biggest uncertainty in this model is the total time for emplacement of Maaz, and in particular, the time between the emplacement of Artuby and Rochette and emplacement of the later Maaz flows. The Maaz members all share similar mineralogy and geochemistry that could be consistent with a shared magma source, so a relatively short time for their overall emplacement is possible. But the erosion and other topographic modifications of the floor outlined above prior to emplacement of Roubion, Nataani, and Chal suggest that some significant

time passed after emplacement of Artuby/Rochette. Furthermore, Roubion itself shows evidence for the development of a weathering profile, and spheroidal weathering has been tentatively identified on Nataani as well (Crumpler et al., this issue), possibly suggesting the presence of one or more weathered paleosurfaces within the Maaz stratigraphy and thus some significant time between flows.

Because of these uncertainties, we cannot rule out that upper Maaz could have been emplaced quite late in the history of Jezero, possibly even postdating lake activity and erosion of the sedimentary cover. While lower Maaz appears to underlie the current delta formation and thus must predate fluviolacustrine activity, upper Maaz does not underlie the delta or any sedimentary remnants on the floor and thus could postdate those deposits. Indeed, these units could be absent near the delta because of the presence of partially eroded delta/lake sediments during their emplacement. Analysis of the alteration history of returned samples could help constrain the degree of aqueous interaction lower vs. upper Maaz experienced and thus their exposure to lake activity.

6.5 Relationship to regional units

The Seitah formation may be related to the regionally extensive Nilli Fossae olivine-bearing unit (Mandon et al., 2020; Brown et al., 2020; Wiens et al., 2022; Beyssac et al., this volume). The regional unit exhibits similar spectral signatures, production of coarse olivine sand grains, and fine-scale layering as Seitah, but drapes underlying topography and thus may be more consistent with a tephra or other clastic deposit rather than an olivine cumulate or other effusive or intrusive deposit (Kremer et al., 2019). As such, it is unclear whether the Seitah cumulates and the regional unit are part of the same deposit, different volcanic deposits from the same magma source (e.g., explosive vs. effusive eruptions from the same vent), different volcanic deposits within a larger regional volcanic complex (e.g., from different vents fed by the same magma bodies or reservoirs), or totally different deposits (e.g., cumulate vs. aeolian deposit).

Likewise, lower Maaz is spectrally and morphologically similar to the regional pyroxene-bearing Capping Unit (Hundal et al., 2022), which is an extensive cratered unit that drapes topography and thus is also interpreted as a tephra deposit. Notably, the capping unit always overlies the Seitah-like regional olivine/carbonate-bearing unit, suggesting a genetic link. In light of these observations, there may be a closer link between Artuby and Seitah than is currently apparent from our in situ data. These regional units are major targets for Perseverance once the rover leaves Jezero crater to explore Nili Planum (Sun & Stack, 2020), so comparison of in situ data from the Capping Unit to the Maaz and Seitah formations will provide important context for the origin of the Jezero crater floor.

Upper Maaz members do not have clear relationships to previously identified regional units, but may provide insight into an enigmatic global class of rocks

with similar CRISM feldspar signatures (Carter and Poulet, 2013; Wray et al., 2013; Viviano-Beck et al., 2017; Rogers & Farrand, 2022). Some of these signatures have been attributed to coarse feldspar in basaltic to basaltic andesite lava flows (Rogers and Nekvasil, 2015), consistent with our observations of upper Maaz, while others have been attributed to exposure of feldspar-rich evolved early crust (Phillips et al., 2022). A closer comparison of upper Maaz to these other feldspar detections may help constrain their origin.

6.6 Geochronological significance of Maaz formation samples

Geochronological analysis of Maaz formation samples after Mars Sample Return will help quantify the timeline described above, by quantifying any potential hiatus in the timing of crystallization between Rochette and Chal member samples. Crater densities suggest that the timescale of erosion of the lake sediments was on the order of hundreds of millions of years, at a minimum (Quantin-Nataf et al., this issue). For example, if the samples are close in age (say, within 10^3 or 10^4 years), this probably implies that all of the Maaz formation pre-dated lake activity, as described in the most likely timeline above, but separations of a hundred million years or more may suggest a more complex emplacement history.

The absolute crystallization ages of the Maaz samples will also be critical for addressing broader questions about the timing of major events in the Jezero region and possibly globally. The crystallization age of the Rochette sample will place an important upper bound on the timing of fluvial activity in Jezero. Estimates for the main pulse of fluvial activity in the Jezero watershed have suggested a Late Noachian age consistent with the peak of global valley network activity (Fassett and Head, 2005), but more recent analyses have suggested that the lower portion of the watershed was reactivated at a later date, possibly in the Hesperian (Mangold et al., 2020). It is currently unclear which period of fluvial activity the bulk of the delta deposits were emplaced by (Mangold & Gupta et al., 2021), but the age of Rochette samples help constrain this by placing an upper bound on the timing of the delta.

In addition, the crystallization age of Chal returned samples may help better constrain the martian cratering chronology, although the complex and extended exhumation history of the crater floor will make this connection challenging. Previous estimates for the age of the crater floor have included 1.4, 3.45 +0.12/-0.67 , and 2.6 $\pm$ 0.5 Ga (Schon et al., 2012; Goudge et al., 2015; Shahrzad et al., 2019), where the range of ages is largely due to inclusion or exclusion of a small number of larger craters in the dataset. More recently, Quantin-Nataf et al. (this issue) showed that the strong gradient in crater density on the floor, which increases away from the delta, is consistent with gradual lateral exhumation of lake sediments on the crater floor toward the delta, resulting in higher crater densities in the floor units to the east that were exposed earlier. If a lateral progression in exhumation began >3 Ga and extended to present day, this

scenario could predict an average crater retention age of ~2.5 Ga, which would be consistent with spatially-averaged crater densities observed across the Jezero floor (Shahrzad et al., 2019; Quantin-Nataf et al., this issue). Results from our study further complicate the interpretation, as we postulate that different members within Maaz also have very different crater retention properties.

However, from this study, Chal represents a rare example of a unit on the crater floor with well-defined boundaries and preserved craters, so more detailed analyses of its crater population along with knowledge of its crystallization age may shed light on the emplacement, burial, and exhumation history of the crater floor. Refinement of these models may provide constraints on the martian cratering chronology, especially if they can be supplemented by additional samples from other geochronological targets beyond the crater floor, most notably including the regional olivine/carbonate-bearing unit, which also has a well-defined crater retention age (Mandon et al., 2020). Additional samples from the rim of Jezero crater and megabreccia in the surrounding plains may also further aid in dating the Jezero and Isidis impacts, which would be important data points in the global cratering chronology.

7. Conclusions

The Jezero crater floor represents the first major geologic terrain investigated and sampled by the Perseverance rover, and samples from the Maaz formation on the crater floor will provide an important geochronological framework for the timing of events in Jezero crater.

Lava flows are a key target for Mars Sample Return due to their high potential for investigations of their geochronology, petrology, and alteration history (iMOST, 2019). In this study, we found that the Maaz formation is consistent with a series of ancient lava flows, with different morphological expressions and spectral properties, which we have used to map their extent in orbital data. The Maaz formation can generally be split into two groups of members based on outcrop expression, spectral properties, composition, and distribution. The lower Maaz members (Artuby/Rochette members) are responsible for the smooth surfaces, lobate margins, and CPX signatures common across the crater floor. In contrast, the upper Maaz members exhibit rough surfaces and possible feldspar signatures that can be mapped to a well-defined lava flow extending southeast from the landing site. The bulk composition of Maaz evolved over time from highly mafic at the base to basaltic andesite at the top, and the overall similarity in mineralogy and composition across Maaz is consistent with a shared and evolving magma source. However, the evolution of the Jezero crater floor through time was complex, and likely included episodes of erosion, tectonic modification, burial by lake sediments, weathering, and exhumation, that occurred both before and after emplacement of the Maaz formation as well as in between emplacement of the upper and lower Maaz members.

We find that the two unique samples collected by Perseverance within the Maaz formation are representative of these upper and lower members, and will allow us to directly test hypotheses for the sequence of events in Jezero crater, including the onset of fluvial activity and the exhumation history of the crater floor. The upper Maaz members retain craters and thus we may be able to link their samples to the global cratering chronology; however, this relationship is not straightforward given the complex history of deposition, topographic modification, and erosion of the crater floor.

8. Acknowledgements

We would like to thank all members of the Mars 2020 science, operations, and engineering teams who made this paper possible, with special thanks to Justin Maki, Bethany Ehlmann, and Kevin Hand. The authors are especially grateful to the Mastcam-Z, SuperCam, and RIMFAX operations teams for their investment in the mission.

Funding: BH, MR, BG, JB, JJ, JN, CM, MSC, ER, and SF were funded by NASA's Mars 2020 Project via a subcontract from the California Institute of Technology/Jet Propulsion Laboratory to Arizona State University (subcontract 1511125). The NASA Mars 2020 Participating Scientist program funded AU (80NSSC21K0330), LC (80NSSC21K0327), and NT. SA and TB were funded by the Swedish Research Council (grant #2017-06388). HA and SEH were funded by the Research Council of Norway (grant 309835, 301238). KK was supported by the Carlsberg Foundation (grant CF19-0023). LM was supported by CNES, CNRS and IRIS OCAV. MM was supported by the EU's Horizon 2020 research and innovation programme under the Marie Skłodowska-Curie grant (No 801199). JS, BC, and DS were funded by the NASA Return Sample Science Participating Scientist Program. AV was funded by NASA (agreement 80HQTR20T0096). AB and GP were funded by ESA PRODEX Contract (PEA 4000117520). EC was funded by the Canadian Space Agency (Grant 22EXPCO14) and the Natural Sciences and Engineering Research Council of Canada (Grant RGPIN-2021-02995). DF was funded by the Australian Research Council (Grant DE210100205). SG was funded by the Royal Society Leverhulme Trust Senior Research Fellowship (SRF\R1\21000106) and the UK Space Agency (grants ST/X002373/1, ST/S001492/1). YL was funded by NASA grant 80NM0018D0004 through JPL. CQN was supported by CNES.

Data availability: The data in this publication are from the Mastcam-Z, RIMFAX, SuperCam, and SHERLOC/Watson instruments on the Mars 2020 Perseverance rover, as well as data from the CRISM and HiRISE instruments on Mars Reconnaissance Orbiter. All image data presented here from Mastcam-Z, WATSON, RIMFAX, CRISM, and HiRISE are available through the Planetary Data System Imaging Node (https://pds-imaging.jpl.nasa.gov/portal/mars2020_mission.html) and Geosciences Node (https://pds-geosciences.wustl.edu/missions/mars2020/). The

Mastcam-Z multispectral database from sols 0-380 is published in Rice et al. (2022b), which includes all Mastcam-Z spectra shown here. Software packages used for Mastcam-Z image processing, spectral extraction, and statistical analyses are part of the open source 'marslab' suite by Million Concepts, LLC: https://zenodo.org/badge/latestdoi/498892781. The SuperCam major element oxide composition (MOC), total emissivity, and all raw data and processed calibrated data files are included in the Planetary Data System (Wiens and Maurice, 2021). SuperCam average chemistry data for the Maaz members is available in Udry et al. (2022).

9. References

Crater floor special issue references:

Alwmark, S. et al. (this issue) Varied origins of Artuby signals complex series of geologic events in Jezero crater, Mars, Journal of Geophysical Research – Planets, submitted.

Beyssac, O. et al. (this issue) Petrological traverse of an olivine-pyroxene cumulate on the floor of Jezero Crater, Mars : a perspective from SuperCam onboard Perseverance, Journal of Geophysical Research – Planets, submitted.

Brown, A. et al. (this issue) Properties of the Nili Fossae Olivine-clay-carbonate lithology: orbital and in situ at Séítah, Journal of Geophysical Research – Planets, submitted.

Casademont et al. (this issue) Dielectric permittivity and density of the shallow Martian subsurface in Jezero Crater, Journal of Geophysical Research – Planets, submitted.

Crumpler, L. et al. (this issue) In Situ Geologic Mapping Transect Observations on the Jezero Crater Floor from Perseverance Rover, Journal of Geophysical Research – Planets, submitted.

Garczynski, B. et al. (this issue) Rock coatings as evidence of later stage aqueous processes at Jezero crater, Mars, Journal of Geophysical Research – Planets, submitted.

Mandon, L. et al. (this issue) Reflectance of Jezero crater floor: 2. Mineralogical interpretation

Merusi, M. et al. (this issue) The Mastcam-Z Radiometric Calibration Targets on NASA's Perseverance Rover: Derived Irradiance Time-Series, Dust Deposition, and Performance over the First 350 Sols on Mars, Journal of Geophysical Research – Planets, submitted.

Quantin-Nataf, C. et al. (this issue) The Complex Exhumation History of Jezero Crater Floor Unit., Journal of Geophysical Research – Planets, submitted.

Rice, M. et al. (this issue) Spectral variability of rocks and soils on the Jezero crater floor: A summary of multispectral observations from Perseverance's Mastcam-Z instrument

Simon, J. et al. (this issue) The First Samples Collected by the NASA Perseverance Rover Mission, Journal of Geophysical Research – Planets, submitted.

Sun, V. et al. (this issue) Exploring the Jezero Crater Floor: Summary and Synthesis of Perseverance's First Science Campaign, Journal of Geophysical Research – Planets, submitted.

Udry, A. et al. (this issue) A Mars 2020 Perseverance SuperCam Perspective on the Igneous Nature of the Máaz formation at Jezero crater, Mars. Journal of Geophysical Research – Planets, submitted.

Vaughan, A. et al. (this issue) Regolith of the crater floor units, Jezero crater, Mars: Textures, composition, and implications for provenance. Journal of Geophysical Research – Planets, submitted.

Other references:

Adams, J. B., & Goullaud, L. H. (1978). Plagioclase feldspars - Visible and near infrared diffuse reflectance spectra as applied to remote sensing. *IN: Lunar and Planetary Science Conference*, *9*, 2901–2909.

Bell, J. F., Maki, J. N., Mehall, G. L., Ravine, M. A., Caplinger, M. A., Bailey, Z. J., et al. (2021). The Mars 2020 Perseverance Rover Mast Camera Zoom (Mastcam-Z) Multispectral, Stereoscopic Imaging Investigation. *Space Science Reviews*, *217*(1), 24. https://doi.org/10.1007/s11214-020-00755-x

Bishop, J. L., Loizeau, D., McKeown, N. K., Saper, L., Dyar, M. D., Marais, D. J. D., et al. (2013). What the ancient phyllosilicates at Mawrth Vallis can tell us about possible habitability on early Mars. *Planetary and Space Science*, *86*, 130–149. https://doi.org/10.1016/j.pss.2013.05.006

Brown, A. J., Viviano, C. E., & Goudge, T. A. (2020). Olivine-Carbonate Mineralogy of the Jezero Crater Region. *Journal of Geophysical Research: Planets*, *125*(3), e2019JE006011. https://doi.org/10.1029/2019je006011

Carli, C., Serventi, G., & Sgavetti, M. (2015). VNIR spectral characteristics of terrestrial igneous effusive rocks: mineralogical composition and the influence of texture. *Geological Society, London, Special Publications*, *401*(1), 139–158. https://doi.org/10.1144/sp401.19

Carli, Cristian, & Sgavetti, M. (2011). Spectral characteristics of rocks: Effects of composition and texture and implications for the interpretation of planet surface compositions. *ICARUS*, *211*(2), 1034–1048.

Carter, J., & Poulet, F. (2013). Ancient plutonic processes on Mars inferred from the detection of possible anorthositic terrains. *Nature Geoscience*, *6*(12), 1008–1012. https://doi.org/10.1038/ngeo1995

Cheek, L. C., & Pieters, C. M. (2014). Reflectance spectroscopy of plagioclase-dominated mineral mixtures: Implications for characterizing lunar anorthosites remotely. *American Mineralogist*, *99*(10), 1871–1892. https://doi.org/10.2138/am-2014-4785

Cloutis, E. A., & Gaffey, M. J. (1991a). Pyroxene spectroscopy revisited - Spectral-compositional correlations and relationship to geothermometry. *Journal of Geophysical Research (ISSN 0148-0227)*, *96*, 22809.

Cloutis, E. A., & Gaffey, M. J. (1991b). Spectral-compositional variations in the constituent minerals of mafic and ultramafic assemblages and remote sensing implications. *Earth Moon And Planets*, *53*, 11–53.

Farley, K.A. et al. (2020). Mars 2020 mission overview. Space Science Reviews, 216(8), 1-41.

Farley, K.A. et al. (2022). Aqueously altered igneous rocks sampled on the floor of Jezero crater, Mars. Science, eabo2196.

Fassett, C. I., & Head, J. W. (2005). Fluvial sedimentary deposits on Mars: Ancient deltas in a crater lake in the Nili Fossae region. *Geophysical Research Letters*, *32*(14), n/a-n/a. https://doi.org/10.1029/2005gl023456

Goudge, T. A., Mustard, J. F., Head, J. W., Fassett, C. I., & Wiseman, S. M. (2015). Assessing the mineralogy of the watershed and fan deposits of the Jezero crater paleolake system, Mars. *Journal of Geophysical Research: Planets*, *120*(4), 775–808. https://doi.org/10.1002/2014je004782

Haber, J. T., Horgan, B., Fraeman, A. A., Johnson, J. R., Bell, J. F., Rice, M. S., et al. (2022). Mineralogy of a possible ancient lakeshore in the Sutton Island member of Mt. Sharp, Gale crater, Mars, from Mastcam multispectral images. Journal of Geophysical Research: Planets, 127, e2022JE007357. https://doi.org/10.1029/2022JE007357

Hamran, S. E. et al. (2020). Radar imager for Mars' subsurface experiment—RIMFAX. Space Science Reviews, 216(8), 1-39.

Hayes, A. G. et al. (2021). Pre-flight calibration of the Mars 2020 Rover Mastcam Zoom (Mastcam-Z) multispectral, stereoscopic imager. Space science reviews, 217(2), 1-95.

Holm-Alwmark, S., Kinch, K. M., Hansen, M. D., Shahrzad, S., Svennevig, K., Abbey, W. J., et al. (2021). Stratigraphic Relationships in Jezero Crater, Mars: Constraints on the Timing of Fluvial-Lacustrine Activity From Orbital Observations. *Journal of Geophysical Research: Planets*, *126*(7). https://doi.org/10.1029/2021je006840

Horgan, B. H. N., Cloutis, E. A., Mann, P., & Bell, J. F. (2014). Near-infrared spectra of ferrous mineral mixtures and methods for their identification in planetary surface spectra. *Icarus*, *234*, 132–154. https://doi.org/10.1016/j.icarus.2014.02.031

Horgan, B. H. N., Johnson, J. R., Fraeman, A. A., Rice, M. S., Seeger, C., Bell, J. F., et al. (2020). Diagenesis of Vera Rubin Ridge, Gale Crater, Mars, From Mastcam Multispectral Images. *Journal of Geophysical Research: Planets*, *125*(11), e2019JE006322. https://doi.org/10.1029/2019je006322

Horgan, B. H. N., Anderson, R. B., Dromart, G., Amador, E. S., & Rice, M. S. (2020). The mineral diversity of Jezero crater: Evidence for possible lacustrine carbonates on Mars. *Icarus*, *339*, 113526. https://doi.org/10.1016/j.icarus.2019.113526

Hundal, C. B., Mustard, J. F., Kremer, C. H., Tarnas, J. D., & Pascuzzo, A. C. (2022). The Circum-Isidis Capping Unit: An Extensive Regional Ashfall Deposit Exposed in Jezero Crater. *Geophysical Research Letters*, *49*(9). https://doi.org/10.1029/2021gl096920

(iMOST), International MSR Objectives and Samples Team, Beaty, D. W., Grady, M. M., McSween, H. Y., Sefton-Nash, E., Carrier, B. L., et al. (2019). The potential science and engineering value of samples delivered to Earth by Mars sample return. *Meteoritics & Planetary Science*, *54*(3), 667–671. https://doi.org/10.1111/maps.13232

Kinch, K. M., Madsen, M. B., Bell, J. F., Maki, J. N., Bailey, Z. J., Hayes, A. G., ... & Winhold, A. (2020). Radiometric calibration targets for the Mastcam-Z Camera on the Mars 2020 Rover mission. Space science reviews, 216(8), 1-51.

Klima, R. L., Dyar, M. D., & Pieters, C. M. (2011). Near-infrared spectra of clinopyroxenes: Effects of calcium content and crystal structure. *Meteoritics & Planetary Science*, *46*(3), 379–395. https://doi.org/10.1111/j.1945-5100.2010.01158.x

Kremer, C. H., Mustard, J. F., & Bramble, M. S. (2019). A widespread olivine-rich ash deposit on Mars. *Geology*, *47*(7), 677–681. https://doi.org/10.1130/g45563.1

Kokaly, R.F., Clark, R.N., Swayze, G.A., Livo, K.E., Hoefen, T.M., Pearson, N.C., Wise, R.A., Benzel, W.M., Lowers, H.A., Driscoll, R.L., and Klein, A.J., 2017, USGS Spectral Library Version 7: U.S. Geological Survey Data Series 1035, 61 p., https://doi.org/10.3133/ds1035.

Liu, Y., et al. (2022). An olivine cumulate outcrop on the floor of Jezero crater, Mars. Science, eabo2756.

Mandon, L., et al. (2020). Refining the age, emplacement and alteration scenarios of the olivine-rich unit in the Nili Fossae region, Mars. Icarus, 336, 113436.

Mangold, N., Dromart, G., Ansan, V., Salese, F., Kleinhans, M. G., Massé, M., ... & Stack, K. M. (2020). Fluvial regimes, morphometry, and age of Jezero crater paleolake inlet valleys and their exobiological significance for the 2020 Rover Mission Landing Site. Astrobiology, 20(8), 994-1013.

Mangold, N., Gupta, S., Gasnault, O., Dromart, G., Tarnas, J. D., Sholes, S. F., ... & Williford, K. H. (2021). Perseverance rover reveals an ancient delta-lake system and flood deposits at Jezero crater, Mars. Science, 374(6568), 711-717.

Mangold, N., Gupta, S., Gasnault, O., Dromart, G., Tarnas, J. D., Sholes, S. F., ... & Williford, K. H. (2021). Perseverance rover reveals an ancient delta-lake system and flood deposits at Jezero crater, Mars. Science, 374(6568), 711-717.

Mcewen, A. S., Eliason, E. M., Bergstrom, J. W., Bridges, N. T., Hansen, C. J., Delamere, W. A., et al. (2007). Mars Reconnaissance Orbiter's High Resolution Imaging Science Experiment (HiRISE). *Journal of Geophysical Research*, *112*(E).

Moeller, R. C., Jandura, L., Rosette, K., Robinson, M., Samuels, J., Silverman, M., ... & Biesiadecki, J. (2021). The Sampling and Caching Subsystem (SCS) for the scientific exploration of Jezero crater by the Mars 2020 Perseverance rover. Space Science Reviews, 217(1), 1-43.

Morris, R. V., Lawson, C. A., Gibson, E. K. J., Lauer, H. V. J., Nace, G. A., & Stewart, C. (1985). Spectral and other physicochemical properties of submicron powders of hematite (alpha-Fe2O3), maghemite (gamma-Fe2O3), magnetite (Fe3O4), goethite (alpha-FeOOH), and lepidocrocite (gamma-FeOOH). *Journal of Geophysical Research (ISSN 0148-0227)*, *90*, 3126–3144.

Murchie, S., Arvidson, R., Bedini, P., Beisser, K., Bibring, J.-P., Bishop, J., et al. (2007). Compact Reconnaissance Imaging Spectrometer for Mars (CRISM) on Mars Reconnaissance Orbiter (MRO). *Journal of Geophysical Research*, *112*(E).

Phillips, M. S., Viviano, C. E., Moersch, J. E., Rogers, A. D., McSween, H. Y., & Seelos, F. P. (2022). Extensive and ancient feldspathic crust detected across north Hellas rim, Mars: Possible implications for primary crust formation. *Geology*. https://doi.org/10.1130/g50341.1

Ravanis, E., Fagents, S., Newman, C., Horgan, B., Holm-Alwmark, S., Brown, A. J., ... & Zorzano, M. P. (2022). The Potential for Pyroclastic Deposits in the Jezero Crater Region of Mars from Ash Dispersal Modeling. 53rd Lunar and Planetary Science Conference, #1692.

Rice, M. S., Seeger, C., Bell, J., Calef, F., St. Clair, M., Eng, A., ... & Wellington, D. (2022). Spectral Diversity of Rocks and Soils in Mastcam Observations Along the Curiosity Rover's Traverse in Gale Crater, Mars. Journal of Geophysical Research: Planets, 127(8), e2021JE007134.

Rice, M. S., Johnson, J. R., Million, C. C., St. Clair, M., Horgan, B. N., et al. (2022b). Mastcam-Z multispectral database from the Perseverance rover's traverse in the Jezero crater floor, Mars (sols 0-380). WWU Geology Faculty Publications, 105, https://doi.org/10.25710/bhyk-kc32.

Rogers, A. D., & Farrand, W. H. (2022). Spectral evidence for alkaline rocks and compositional diversity among feldspathic light-toned terrains on Mars. *Icarus*, *376*, 114883. https://doi.org/10.1016/j.icarus.2022.114883

Rogers, A. D., & Nekvasil, H. (2015). Feldspathic rocks on Mars: Compositional constraints from infrared spectroscopy and possible for-

mation mechanisms. *Geophysical Research Letters*, *42*(8), 2619–2626. https://doi.org/10.1002/2015gl063501

Rudolph, A., et al. (2022). The distribution of clay minerals and their impact on diagenesis in Glen Torridon, Gale crater, Mars. Journal of Geophysical Research: Planets, e2021JE007098.

Schade, U., Wasch, R., & Moroz, L. (2004). Near-infrared reflectance spectroscopy of Ca-rich clinopyroxenes and prospects for remote spectral characterization of planetary surfaces. *ICARUS*, *168*(1), 80–92.

Schon, S. C., Head, J. W., & Fassett, C. I. (2012). An overfilled lacustrine system and progradational delta in Jezero crater, Mars: Implications for Noachian climate. *Planetary and Space Science*, *67*(1), 28–45. https://doi.org/10.1016/j.pss.2012.02.003

Scudder, N. A., Horgan, B. H. N., Rampe, E. B., Smith, R. J., & Rutledge, A. M. (2021). The effects of magmatic evolution, crystallinity, and microtexture on the visible/near-infrared and thermal-infrared spectra of volcanic rocks. *Icarus*, *359*, 114344. https://doi.org/10.1016/j.icarus.2021.114344

Seelos, F. P., Viviano-Beck, C. E., Morgan, M. F., Romeo, G., Aiello, J. J., & Murchie, S. L. (2016). CRISM hyperspectral targeted observation PDS product sets—TERs and MTRDRs. 47th Lunar and Planetary Science Conference, #1783.

Serventi, G., Carli, C., Sgavetti, M., Ciarniello, M., Capaccioni, F., & Pedrazzi, G. (2013). Spectral variability of plagioclase–mafic mixtures (1): Effects of chemistry and modal abundance in reflectance spectra of rocks and mineral mixtures. *Icarus*, *226*(1), 282–298. https://doi.org/10.1016/j.icarus.2013.05.041

Shahrzad, S., Kinch, K. M., Goudge, T. A., Fassett, C. I., Needham, D. H., Quantin-Nataf, C., & Knudsen, C. P. (2019). Crater Statistics on the Dark-Toned, Mafic Floor Unit in Jezero Crater, Mars. *Geophysical Research Letters*, *46*(5), 2408–2416. https://doi.org/10.1029/2018gl081402

St. Clair, M., C. Million, M. Rice (2022) Marslab software suite, https://zenodo.org/badge/latestdoi/498892781.

Stack, K. M., Williams, N. R., Calef, F., Sun, V. Z., Williford, K. H., Farley, K. A., et al. (2020). Photogeologic Map of the Perseverance Rover Field Site in Jezero Crater Constructed by the Mars 2020 Science Team. *Space Science Reviews*, *216*(8), 127. https://doi.org/10.1007/s11214-020-00739-x

Rice, M. S., Seeger, C., Bell, J., Calef, F., St. Clair, M., Eng, A., ... & Wellington, D. (2022). Spectral Diversity of Rocks and Soils in Mastcam Observations Along the Curiosity Rover's Traverse in Gale Crater, Mars. Journal of Geophysical Research: Planets, 127(8), e2021JE007134.

Townsend, T. E. (1987). Discrimination of iron alteration minerals in visible and near-infrared reflectance data. Journal of Geophysical Research: Solid Earth,

92(B2), 1441-1454.

Udry, A. et al. (2022) A Mars 2020 Perseverance SuperCam Perspective on the Igneous Nature of the Máaz formation at Jezero crater and link with Séítah, Mars.Journal of Geophysical Research: Planets. https://doi.org/10.6084/m9.figshare.21038962.

Viviano-Beck, C. E., Seelos, F. P., Murchie, S. L., Kahn, E. G., Seelos, K. D., Taylor, H. W., et al. (2014). Revised CRISM spectral parameters and summary products based on the currently detected mineral diversity on Mars. *Journal of Geophysical Research: Planets*, *119*(6), 1403–1431. https://doi.org/10.1002/2014je004627

Viviano-Beck, C. E., Murchie, S. L., Beck, A. W., & Dohm, J. M. (2017). Compositional and structural constraints on the geologic history of eastern Tharsis Rise, Mars. Icarus, 284, 43-58.

Wiens, R. C. and Maurice, S. (2021). Mars 2020 SuperCam Bundle. NASA Planetary Data System. https://doi.org/10.17189/1522646

Wiens, R. C., Udry, A., Beyssac, O., Quantin-Nataf, C., Mangold, N., Cousin, A., ... & SuperCam Team. (2022). Compositionally and density stratified igneous terrain in Jezero crater, Mars. Science advances, 8(34), eabo3399.

Wray, J. J., Hansen, S. T., Dufek, J., Swayze, G. A., Murchie, S. L., Seelos, F. P., et al. (2013). Prolonged magmatic activity on Mars inferred from the detection of felsic rocks. *Nature Geoscience*, *6*(12), 1013–1017. https://doi.org/10.1038/ngeo1994